Comparative Response Evaluation of two Design Options for Tresfjordbru

Subjected to Seismic Loading

by
Semko Majidian

THESIS

for the degree of

MASTER OF SCIENCE

(Master i Anvendt matematikk og mekanikk)

Faculty of Mathematics and Natural Sciences

UNIVERSITY OF OSLO

27.05.2013

Comparative Response Evaluation of two Design Options for Tresfjordbru

Subjected to Seismic Loading

by
Semko Majidian

THESIS
for the degree of
MASTER OF SCIENCE

(Master i Anvendt matematikk og mekanikk)

Faculty of Mathematics and Natural Sciences
UNIVERSITY OF OSLO

27.05.2013

Det matematisk- naturvitenskapeligakultet
Universitetet i oslo

Abstract

Out of two alternative bridge designs, a cantilever bridge is chosen as a highway bridge by the owner in collaboration with a consulting company. The design decision is based on initial cost estimates and regular maintenance costs without much regard to the potential damage the bridge can sustain due to earthquakes during its economical lifespan and the repair costs.

The main purpose of this thesis is a response evaluation of the two bridge designs subjected to earthquake induced ground motion. As a result of this study, advantages and dis advantages of one of the designs compared to the other from the seismic behavior and seismic point of view will be identified and documented.

The concept of structural dynamics has been the main pillar of this study where principle elements are used to derive the basis of two central methods of analysis and their area of application. The practical elastic response spectrum analysis and its adequate approximate solution is the first main analysis method. The second method of analysis is the time history analysis with its exact solution.

Based on the solutions by both methods of analysis and a demand capacity ratio assessment it can be concluded that none of the designs will enter ductile behavior. However, with regard to comparison of the designs it can be documented that design two is more susceptible to damage during an earthquake.

Acknowledgments

No one walks alone on the journey of life. Just where do I start to thank those that joined you, walked beside you, and helped you along the way.

I owe my sincere gratitude to my supervisor, Dr. Emrah Erduran who was abundantly helpful and offered invaluable assistance, support and guidance. I also would like to thank my wife, for her love, kindness and support she has shown during the past two years it has taken me to finalize this thesis. Furthermore I would like to thank my parents for their endless love and support.

Last but not least, I would like to thank my friend Henning Tyvand, my college Aja Anta Magerøy and all the nice people I met at NORSAR.

Table of Contents

Notation

Roman Symbols

a_0	Coefficient that relate the mass to damping
a_1	Coefficient that relate the stiffness to damping
A_n	Integration constant
B_n	Integration constant
c	Viscous damping coefficient
$\boldsymbol{c}$	Damping matrix
c_{cr}	Critical damping coefficient
E_S	Young's modulus for steel
E	Young's modulus for concrete
F	General force
f_n	Natural cyclic frequency of vibration
f_I	Inertia force
f_D	Damping force
f_S	Elastic force
f_{yk}	Characteristic yield strength for steel
f_{ck}	Cylinder strength for concrete
$\boldsymbol{f(t)}$	Total element force (vector)
$\boldsymbol{f_n(t)}$	The *n*th mode contribution of an element (vector)
k	Structural stiffness
$\boldsymbol{k}$	Stiffness matrix
K_n	Generalized stiffness for the *n*th mode
k_T	Transverse stiffness
k_L	Longitadinal stiffness
L	Love waves
m	Mass
$\boldsymbol{m}$	Mass matrix

M_n	Generalized mass for the nth mode
$\boldsymbol{M_n}$	Spectral mass matrix
P	Pressure waves
$p(t)$	External dynamic force
$P_n(t)$	Generalized force for the nth mode
P_{NCR}	Probability of exceedance of 10% in 50 years
q	Behavior factor
$q_r(t)$	Modal coordinate for the rth mode
$\boldsymbol{q(t)}$	Modal coordinates (vector)
$q_n(t)$	Modal coordinate for the nth mode
R	Rayleigh waves
S_e	Spectral acceleration of RS or DS in units of g
S	Shear waves
$\boldsymbol{s}$	Spatial distribution (vector)
$\boldsymbol{s_n}$	Spatial contribution for the nth mode
T_{NCR}	Reference return period
T_n	Natural period of vibration for the nth mode
T_D	Natural period of a damped system
$\ddot{\boldsymbol{u}}$	Acceleration (vector)
$\dot{\boldsymbol{u}}$	Velocity (vector)
$\boldsymbol{u}$	Displacement (vector)
$\boldsymbol{u_s}$	Quasi-static displacement
$\boldsymbol{u(t)}$	Relative displacement
$\ddot{u}_g(t)$	Ground acceleration
$\ddot{u}$	Acceleration
$\dot{u}$	Velocity
u	Relative displacement
u_t	Total displacement
u_g	Ground displacement

u_p	Peak displacement
$u(t)$	Complete solution of the linear differential equation of motion
$u_c(t)$	Complementary solution
$u_p(t)$	Particular solution
$u(0)$	Initial displacement
$\boldsymbol{u_n(t)}$	Displacement for the nth mode (vector)
u_T	Transverse displacement
u_L	Longitadinal displacement
v	Poisson's ratio

Greek Symbols

τ	Dummy time variable in duhamel's integral
ζ	Damping ratio
ζ_n	Damping ratio for the nth mode
ω_n	Natural circular frequency of vibration
$\boldsymbol{\phi_n}$	Mode shape for the nth mode (vector)
$\boldsymbol{\phi_r}$	Mode shape for the rth mode (vector)
Γ_n	Mass Participation factor for the nth mode
γ_I	Importance factor
β	parameter in Newmark's method
γ	parameter in Newmark's method

Abbreviations

DOF	Degree of freedom
SDOF	Single degree of freedom
MDOF	Multi degree of freedom
ULS	Ultimate limit state
ALS	Accident limit state
RSA	Response spectrum analysis
THA	Time history analysis
DSA	Design spectrum analysis

1 Introduction

1.1 Motivation

Despite their structural simplicity, bridges are among structures that are particularly vulnerable to earthquakes. Little or no structural redundancy, soil-structure sensitivity, lack of adequate design philosophy are among many other reasons of poor bridge performance witnessed around the world during earthquakes. However, because of a very low probability of earthquake occurrence on Norwegian soil with significant magnitude, it is very hard to get a feeling on how existing or future bridge structures will perform when the unthinkable event strikes. And so, despite the mandatory implementation of Eurocode 8, design decisions are generally based on initial cost estimates without much regard to the potential damage the bridge can sustain due to earthquakes.

As I forthcoming engineer, I like to understand the technical impact of earthquake on important and complicated structures. And by learning and understanding application methods, it may give me the opportunity and ability to benefit society by saving life and money.

1.2 Specifications

The following objectives will be accomplished

1. With the use of OpenSees and Matlab seven response spectrums for seven selected ground motions will be constructed. By following the guidelines of Eurocode 8, the response spectrums will be scaled to level up with the Seismic Zonation of Norway.

2. Two alternative bridge designs will be modeled in NovaFrame with appropriate assumptions. The models will get subjected to previous scaled ground motions and be analyzed by the method of response spectrum analysis (RSA). The models will also be analyzed and partly designed following the guidelines of obtaining and applying the design spectrum.

3. The two bridge designs will be modeled in OpenSees by the same assumptions of the previous modeling in NovaFrame. Both designs will be analyzed under seven scaled ground motions by the method of time history analysis (THA).

4. Structural response of the two bridge designs analyzed by the presiding methods will be compared and evaluated with respect to eigenvalues, modal participation, flexural strength and displacements.

5. Assessment of the bridge designs will be evaluated. The moment demands from the THA by OpenSees will be compared to the strength capacity of the two designed in NovaFrame with respect to the design spectrum. The assessment along with the preceding evaluation will be the bases of a total comparison of the two designs.

1.3 Outline

This thesis consists of in total 8 chapters.

Chapter 2 provides some of the necessary theoretical background needed to understand the complexity of the specifications in this thesis. Concepts of structural dynamics are introduced. By following simpler bridge models the thesis is organized to facilitate dynamic applications toward the actual designs.

Chapter 3 unlocks some of the basic concepts of earthquakes. Understanding ground motion, quantification and relation to structural dynamics.

Chapter 4 presents the numerical modeling.

Chapter 5 and 6 presents the results and discussion of analysis for the longitudinal and transverse directions.

Chapter 7 and 8 is mainly about the assessment of the designs, comparison of designs and conclusion.

2 Theory of structural dynamics

2.1 Introduction

The aim of this chapter is to present basic concepts and assumptions used in dynamic analysis. Later, it will be shown how these analysis methods can be utilized to estimate dynamic behavior of bridges subjected to seismic loading.

2.2 Structural Analysis

To understand how a structure works under various loads, we need to describe its behavior in term of displacements, forces and deformations, which in general form are called structural response. These responses need to be quantified in order to create an optimal and safe design.

In general, structural analysis of ordinary structures can be classified in two types of analysis: Static and Dynamic. The main difference between these two analysis options is the way the loads are defined, which is explicit in the names of the analysis. Static analysis treats loading independent of time. It means that the loading position, magnitude and direction are unchanged, while the position, magnitude or direction of loading in dynamic analysis varies with time.

2.3 Dynamics of SDOF Systems

2.3.1 Introduction

In this section the structural dynamic problem is formulated for a simple bridge structure which will be referred to as sample 1 and can be idealized as a system with a lumped mass and a massless column. Sample 1, which is assumed to be an elastic system, will be subjected to dynamic excitation as well as earthquake induced ground motion in longitudinal direction. Differential equations governing the motion of sample 1 as a SDOF system will be derived and different solution methods will be introduced.

2.3.2 Single Degree of Freedom Systems, SDOF

Structural response of a bridge due to dynamic excitation depends on the mass, damping and stiffness properties of the bridge. The dynamic excitation and response can best be explained by means of a SDOF system model of a simple bridge.

Degree of freedom (DOF) means the number of independent displacements required to define the displaced position of the mass of a structure relative to its original position. A SDOF system indicates that only one independent displacement is needed for the entire structure to describe its mass displacement.

Figure 1(a) shows a simple regular bridge structure (Sample 1) with two spans and one column. The bridge deck is axially rigid and the abutments do not prevent longitudinal displacement. The superstructure is assumed to be infinitely stiff and the longitudinal flexibility of the bridge is due entirely to the column. The column's mass can be neglected as its mass ratio compared to the superstructure is insignificant. Figure 1(b) shows a model representation of Sample 1 in transverse direction. This is a SDOF system with lumped mass.

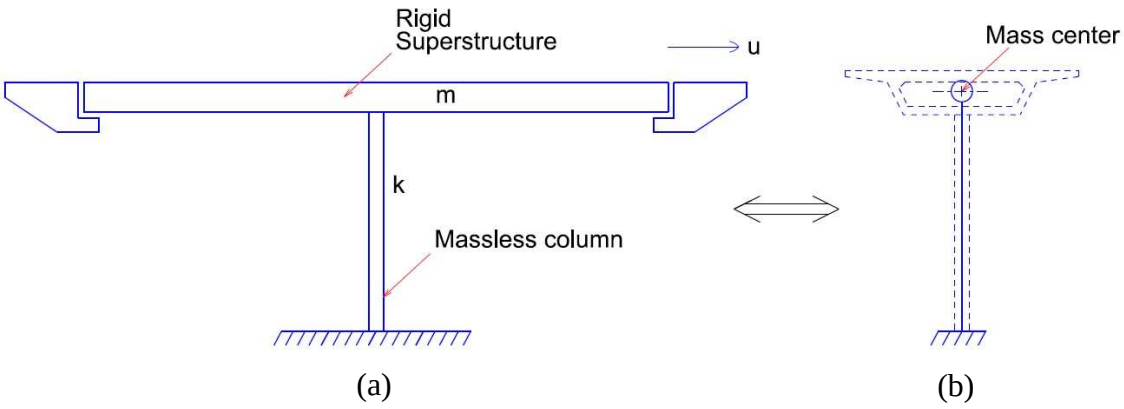

Figure 1 - Overview of a simple bridge (Sample 1)

Figure 2(a) and 2(b) shows two different model representations of Sample 1 in both directions as the total distributed mass of the superstructure is concentrated (lumped) at top of the column at the superstructure section's mass center. In other words figure 2(a) and 2(b) are the SDOF system representations of figure 1 in both longitudinal and transversal where the relevant mass displacement is only defined by one DOF in each direction.

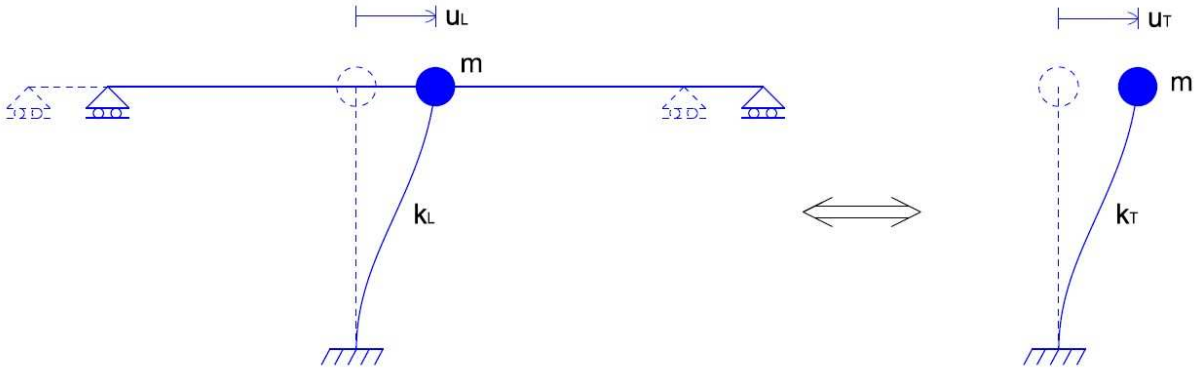

Figure 2 - model representation of Sample 1

2.3.3 Acting Forces, SDOF

When the structure in Sample 1 is excited by an external dynamic force $P(t)$, the structure's internal forces will try to oppose this excitation at a given instant. Internal forces arise due to the structures natural properties when an external force is trying to push it out of its equilibrium position. These forces consist of Inertia (f_I), damping (f_D) and elastic (f_S) forces with the direction shown in figure 3.

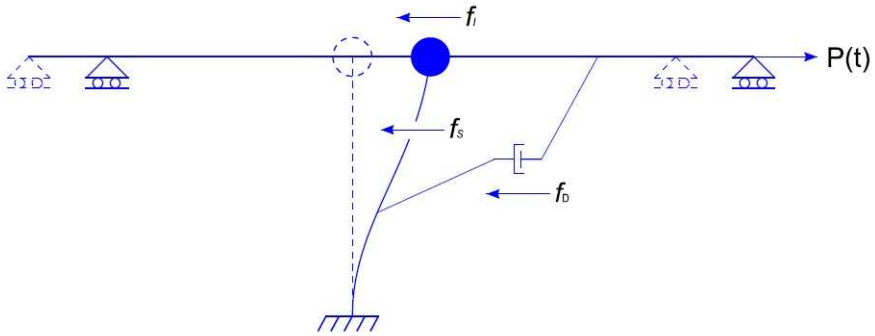

Figure 3 – Overview of internal forces acting on Sample 1 due to P(t)

When an arbitrary object with a mass of m is accelerated, inertial forces are created in the object that will try to oppose this acceleration. The inertial force due to any type of acceleration can be expressed as:

$$f_I = m\ddot{u} \tag{2.3.1}$$

Where f_I denotes the inertial force, m is the mass of the structure and $\ddot{u}$ is the total acceleration of the mass.

Damping is simply a structural characteristic for dissipating energy under vibration. When a structure is excited and begins to vibrate, the structure will try to damp this vibration velocity by different mechanisms to a complete stop. In reality it is impossible to determine the damping force for every type of damping mechanism mathematically and therefore in many practical situations a linear viscous damper is used as an idealized representation. In general the damping force due to any type of velocity can be expressed as:

$$f_D = c\dot{u} \tag{2.3.2}$$

Where f_D denotes the damping force, c is the viscous damping coefficient and $\dot{u}$ is the velocity across the viscous damper.

The structural stiffness properties can be explained as an internal elastic force resisting deformations. It is a relationship between the internal force and the relative displacement of the structure. In general the elastic force due to any type of small deformation can be expressed as:

$$f_S = ku \tag{2.3.3}$$

Where f_S denotes the elastic force, k is the stiffness coefficient and u is the relative displacement associated with deformations in the structure.

2.3.4 Equation of Motion, SDOF

In static analysis the structure can reach its equilibrium position when sum of external forces are equal to the sum of internal forces in the same direction. The structure's internal forces consist of only one type of force which is due to the stiffness properties of varies building materials. When we deal with dynamic analysis we also have to take the inertial and damping effects into consideration. These effects will arise when a structure enters a motion state. By applying Newton's second law of motion and D'

Alembert's principle we can derive a differential equation which will govern the unknown displacements $u(t)$ of the SDOF system.

Using equations 2.3.1 and 2.3.2 the equilibrium condition can be written as:

$$p(t) - f_D - f_S = -f_I \qquad 2.3.4$$

Or

$$\mathrm{m}\ddot{u} + c\dot{u} + ku - p(t) = 0 \qquad 2.3.5$$

Where $p(t)$ is the external dynamic force.

D' Alembert's principle states that by implementing the inertial force to a system, dynamic equilibrium can be obtained at any time instant. Then, 2.3.5 can be rewritten as 2.3.6 which is known as the equation of motion for an elastic SDOF system:

$$m\ddot{u}(t) + c\dot{u}(t) + ku(t) - p(t) = 0 \qquad 2.3.6$$

2.3.5 Equation of Motion Adopted to Earthquake for SDOF System

In this section sample 1 will be exposed to an earthquake induced ground motion by displacement at the base of its column.

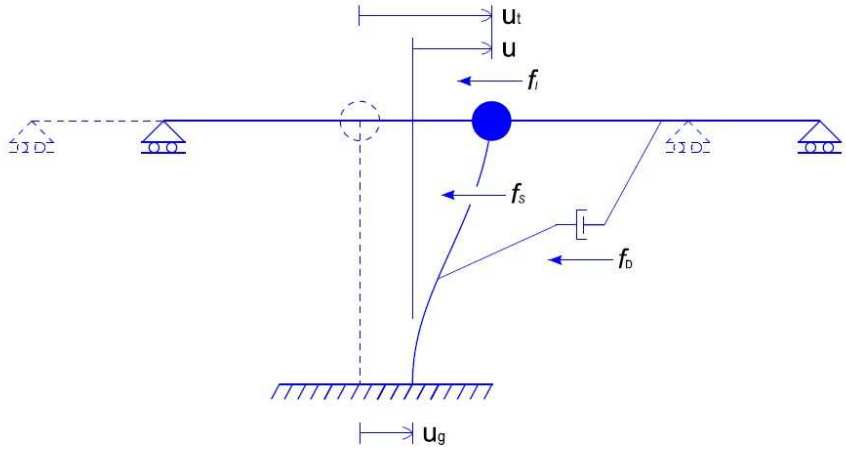

Figure 4 - Sample 1 exposed to ground motion

As illustrated in figure 4, the ground displacement is denoted by u_g, the displacement of the mass relative to the columns base is denoted by u and the total displacement of the mass is denoted by $u_t$which is equal to:

$$u_t(t) = u_g(t) + u(t) \qquad 2.3.7$$

Since sample 1 is now excited by an earthquake and not an external force $p(t)$ as shown in figure 4, the equation of motion has to be modified to consider this new type of excitation.

It is essential to note that only the mass displacement relative to the column base produces elastic and damping forces while the mass's inertial force is related to its total acceleration. This conclusion will lead to the following equation of motion for a SDOF system subjected to ground acceleration:

$$m\ddot{u}_t(t) + c\dot{u}(t) + ku(t) = 0 \qquad 2.3.8$$

where

$$\ddot{u}_t(t) = \ddot{u}_g(t) + \ddot{u}(t) \qquad 2.3.9$$

By substituting equation 2.3.7 in 2.3.8, and using equation 2.3.9, the equation of motion for a SDOF subjected to earthquake can be written as:

$$m\ddot{u}(t) + c\dot{u}(t) + ku(t) = -m\ddot{u}_g(t) \qquad 2.3.10$$

2.3.6 Solution of the differential equation of Motion for a SDOF System

In this section different solution methods along with area of application will be introduced briefly.

Classical Solution

Complete solution of the linear differential equation of motion consists of the sum of the complementary solution $u_c(t)$ and the particular solution $u_p(t)$, that is, $u(t) = u_c(t) + u_p(t)$. Since the differential equation is of second order, two constants of integration are involved. They appear in the complementary solution and are evaluated from a knowledge of the initial conditions.

Duhamel's Integral

Another well-known approach to the solution of linear differential equations, such as the equation of motion of an SDF system, is based on representing the applied force as a sequence of infinitesimally short impulses. The response of the system to an applied force, $p(t)$, at time t is obtained by adding the responses to all impulses up to the time. This will lead to the following equation known as *Duhamel`s integra*l for an undamped SDF system with a natural frequency: $\omega_n(t)$

$$u(t) = \frac{1}{m\omega_n} \int_0^1 p(\tau)\ \sin[\omega_n(t - \tau)]\, d\tau$$

Numerical Methods

The two preceding dynamic analysis methods are restricted to linear systems with harmonic excitations. The analytical solution of the equation of motion is usually not possible when the excitation varies arbitrarily with time. This is the case for analyzing systems subjected to ground motion. The practical approach for such systems is numerical time stepping methods for integration of differential equations with the use of computational calculations as a software tool.

2.3.7 Free Vibration, SDOF

When a SDOF system is disturbed from its static equilibrium position by enforcing an initial displacement and is allowed to oscillate back and forth freely without any external dynamic excitation, this is called natural free vibration. Figure 5 shows a SDOF system with the initial displacement $u(0)$ and the peak displacement, u_p.

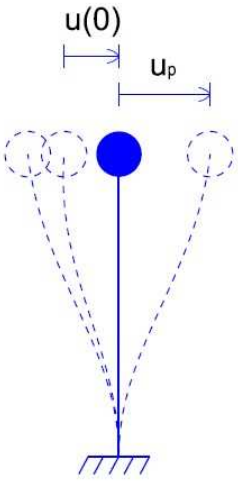

Figure 5 - Free vibration of a SDOF system

2.3.8 Undamped Free Vibration, SDOF

Equation of motion for a SDOF system without damping undergoing free vibration can be expressed as:

$$m\ddot{u}(t) + ku(t) = 0 \qquad 2.3.16$$

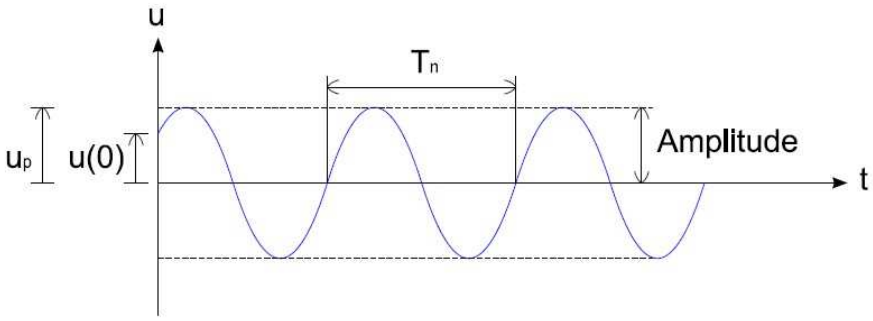

Figure 6 - free vibration of an undamped SDOF system

Every structure has its own natural vibrational characteristics which can be determined mathematically.

By knowing the initial conditions, that is velocity and displacement at time zero, equation 2.3.16 can be solved. The solution to the homogeneous differential equation is obtained by standard methods:

$$u(t) = \mathrm{u}(0)\cos(\omega_n \mathrm{t}) + \frac{\dot{u}}{\omega_n}\omega^2 \sin(\omega_n \mathrm{t}) = 0 \qquad 2.3.17$$

Where

$$\omega^2 = \frac{k}{m} \qquad 2.3.18$$

These natural characteristics, which depend only on the mass and stiffness of the structure, are:

- Natural period of vibration: $T_n = \frac{2\pi}{\omega_n}$ in units of second
- Natural circular frequency of vibration: $\omega_n = \frac{T_n}{2\pi}$ in units of radians per second
- Natural cyclic frequency of vibration: $f_n = \frac{1}{T_n}$ in units of Hz or cycles per second

2.3.9 Damped Free Vibration, SDOF

In reality every structure undergoing free vibration will eventually come to a complete halt and this is due to various damping mechanisms that will arise under motion. Equation of motion for a damped system undergoing free vibration can be expressed as:

$$m\ddot{u}(t) + c\dot{u}(t) + ku(t) = 0 \qquad 2.3.19$$

Figure 7 shows how the free vibration of a SDOF system decaying with time due to damping. The natural period of a damped system $T_D = \frac{2\pi}{\omega_D}$ has a tendency to be longer than the natural period of an undamped system T_n where these are related by $T_D = \frac{T_n}{\sqrt{1-\zeta^2}}$.

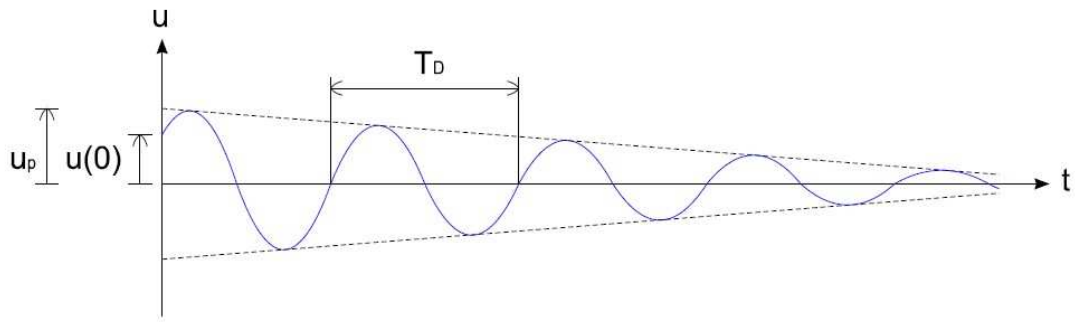

Figure 7 - Free vibration of a Damped SDOF system

2.3.10 Damping Ratio

The damping ratio is a dimensionless measure of damping. It is a system property that depends on its mass and stiffness.

Dividing 2.3.19 by m gives:

$$\ddot{u}(t) + 2\zeta\omega_n\dot{u}(t) + \omega_n^2 u(t) = 0$$

where:

$$\omega_n^2 = \frac{k}{m} \qquad \zeta = \frac{c}{c_{cr}} \qquad c_{cr} = 2m\omega_n$$

ζ denotes the damping ratio which controls how fast the vibration will decay, c is a measure of the energy dissipated in cycle of free or forced harmonic vibration and c_{cr} is the critical damping coefficient which controls the damping limit where the structure will be damped without any oscillation.

2.4 Dynamics of MDOF Systems

2.4.1 Introduction

In this section we deal with discretized systems with a finite number of DOF. By using a two storey simple bridge referred to as sample 2 we will establish stiffness, damping and mass components and derive the equation of motion for a MDOF system.

2.4.2 Multi Degree of Freedom Systems, MDOF

A MDOF system is a system where more than one DOF is required to define the displaced position of all the structure's mass relative to its original position. Solving MDF systems using analytical methods requires a tremendous effort and as DOFs increase the solution becomes more tedious. Therefore computers and numerical analysis are essential tools for managing this task.

Although two storey small bridges are not at all common in reality, there are several known multi span bridges with two storeys carrying car traffic on one storey and a railroad at the other. Figure 8(a) shows a simple two storey bridge structure (Sample 2) with two spans and one column at each storey. The bridge deck is axially rigid and the abutments do not prevent longitudinal displacement. The superstructures are assumed to be infinitely stiff and the longitudinal stiffness of the bridge is due entirely to the columns. The columns mass can be neglected as their mass ratio compared to the superstructure is almost insignificant. Figure 8(b) shows a model representation of Sample 2 in transverse direction. This is a MDOF system with lumped mass at the top of the columns only assuming that the bridge is regular.

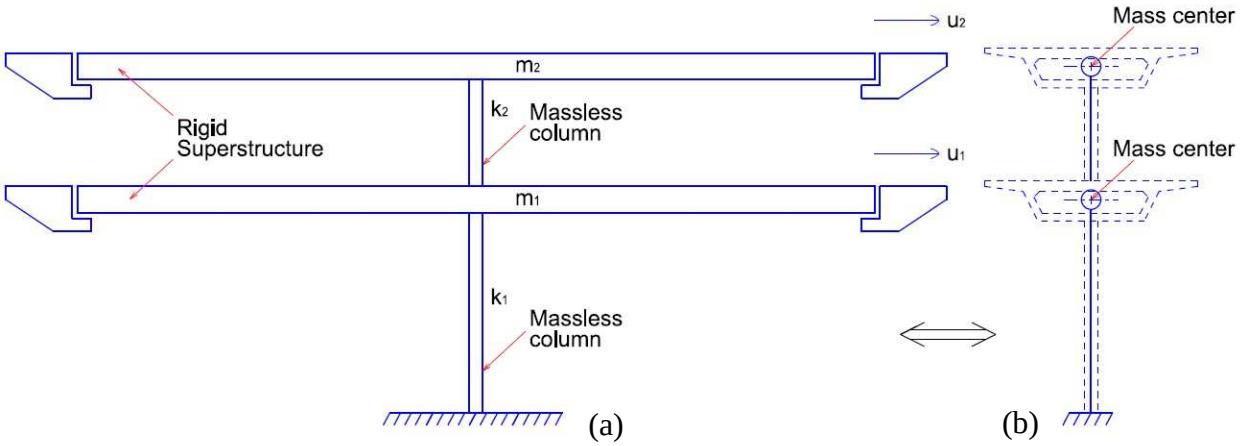

Figure 8 – A two storey bridge shown in longitudinal and transverse direction (Sample 2)

Figure 9(a) and 9(b) shows a model representation of sample 2 in longitudinal and transversal direction as the total distributed mass of each superstructure is concentrated (lumped) at top of the column and at the superstructure section's mass center. In other words figure 9(a) and 9(b) are the MDOF system representations of Sample 2 where the relevant mass displacements are only defined by two DOFs in each direction.

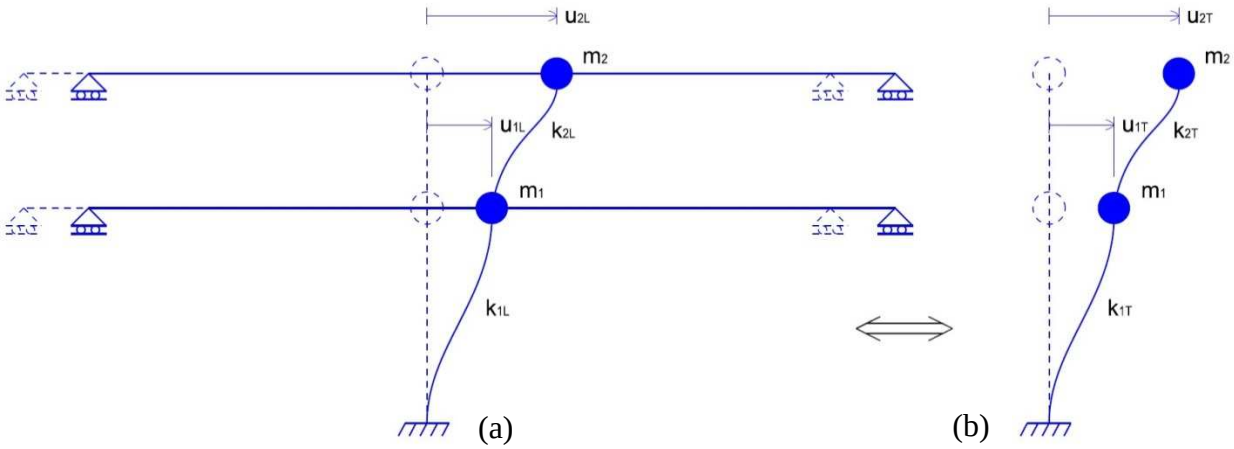

Figure 9 - Model representation of Sample 2

2.4.3 General Modeling approach for a MDOF System

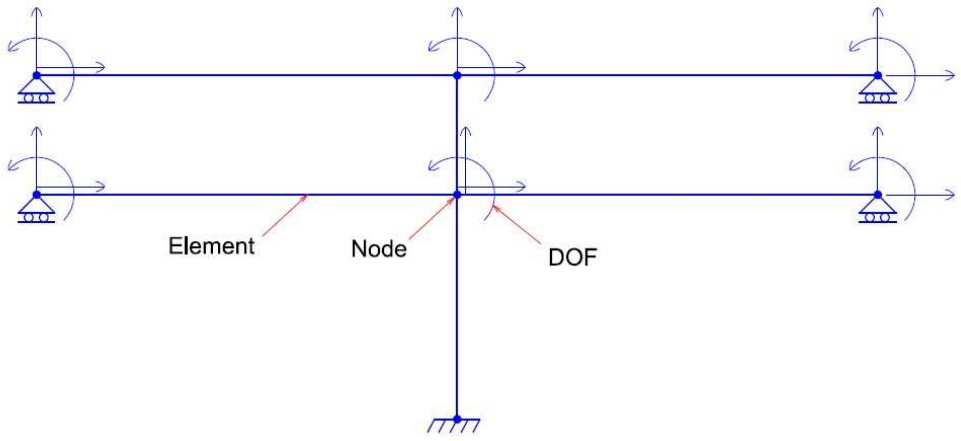

Figure 10 - General DOFs for a 2D model of Sample 2

The above model is a representation of general DOFs for Sample 2. The model consists of elements which represent the structural components and nodes which are connection points for the elements. Figure 10 shows three DOFs at each node. Since this is a 2D model there are two translations and one rotation at each node.

2.4.4 Equation of Motion for a MDOF System

In the same way as for a SDOF system, elastic, damping and inertia forces act as internal forces on the bridge. However, unlike the SDOF system where all forces and displacements are denoted using scalars, for MDOF systems, the displacements and forces are denoted using vectors.

Next, in figure 11 the DOFs required for establishing the equation of motion for sample2 is determined by discretizing the general model in figure 10 where axial deformations as well as node rotations are neglected due to the rigid superstructure. Due to this discretization where all the DOFs except u_1 and u_2 are ruled out, we get the same model representation as figure 9.

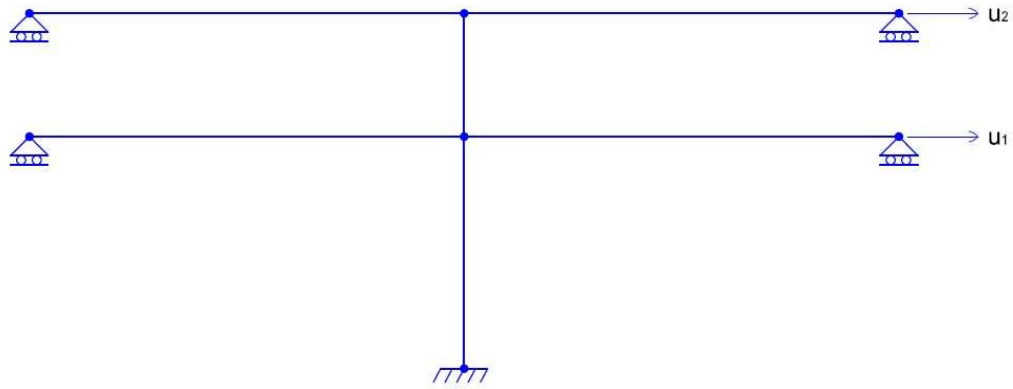

Figure 11 - Two DOFs model of Sample 2 where axial deformation and node rotations are neglected

The equation of Motion for Sample 2 without external excitation (free vibration) can then be written as:

$$[\boldsymbol{m}]\{\ddot{\boldsymbol{u}}(\boldsymbol{t})\} + [\boldsymbol{c}]\{\dot{\boldsymbol{u}}(\boldsymbol{t})\} + [\boldsymbol{k}]\{\boldsymbol{u}(\boldsymbol{t})\} = \boldsymbol{0} \qquad 2.4.1$$

Where $\boldsymbol{m}$, $\boldsymbol{c}$, and $\boldsymbol{k}$ are the mass, damping and stiffness matrices respectively and $\ddot{\boldsymbol{u}}$, $\dot{\boldsymbol{u}}$, and $\boldsymbol{u}$ are the acceleration, velocity and displacement vectors respectively:

$$\begin{bmatrix} \boldsymbol{m_1} & \boldsymbol{0} \\ \boldsymbol{0} & \boldsymbol{m_2} \end{bmatrix} \begin{Bmatrix} \ddot{\boldsymbol{u}}_1 \\ \ddot{\boldsymbol{u}}_2 \end{Bmatrix} + \begin{bmatrix} \boldsymbol{c_{11}} & \boldsymbol{c_{12}} \\ \boldsymbol{c_{21}} & \boldsymbol{c_{22}} \end{bmatrix} \begin{Bmatrix} \dot{\boldsymbol{u}}_2 \\ \dot{\boldsymbol{u}}_2 \end{Bmatrix} + \begin{bmatrix} \boldsymbol{k_{11}} & \boldsymbol{k_{12}} \\ \boldsymbol{k_{21}} & \boldsymbol{k_{22}} \end{bmatrix} \begin{Bmatrix} \boldsymbol{u}_1 \\ \boldsymbol{u}_2 \end{Bmatrix} = \begin{Bmatrix} 0 \\ 0 \end{Bmatrix} \qquad 2.4.2$$

The stiffness matrix can be obtained by superposition and concept of stiffness influence. The mass matrix is also established simply by computing the mass at each bridge deck. On the other hand, establishing the damping matrix is not as straight forward. The method used to establish the damping matrix is explained in the next section.

2.4.5 Rayleigh Damping

Damping is generally specified by numerical values for the modal damping ratio which are sufficient for linear systems with classical damping. The reason for this is the impractical determination of damping coefficients directly from the structure.

Rayleigh damping is a reliable method for constructing a classical damping matrix using modal damping ratios. This approach is an appropriate idealization if similar damping mechanisms are distributed throughout of the structure. Rayleigh damping is expressed as:

$$[\boldsymbol{c}] = a_0[\boldsymbol{m}] + a_1[\boldsymbol{k}] \tag{2.4.3}$$

Where $\boldsymbol{c}$ denotes the damping matrix and a_0 and a_1 are coefficients that relate the mass and the stiffness to damping respectively. The damping ratio for the nth mode is derived as:

$$\zeta_n = \frac{a_0}{2}\frac{1}{\omega_n} + \frac{a_1}{2}\omega_n \tag{2.4.4}$$

Equation 2.4.4 can then be used to determine a_0 and $a_1$and can be transformed to vectors for a MDF system, in this case for sample 2 with two DOFs.

$$\frac{1}{2}\begin{bmatrix} 1/\omega_1 & \omega_1 \\ 1/\omega_2 & \omega_2 \end{bmatrix}\begin{Bmatrix} a_0 \\ a_1 \end{Bmatrix} = \begin{Bmatrix} \zeta_1 \\ \zeta_2 \end{Bmatrix} \tag{2.4.5}$$

Figure 12 shows how the damping ratio for the nth mode can vary with the natural frequency. To ensure reasonable values for the damping ratios in all the modes with the most contribution to the response it is important to choose mode i and j that coincides. Then figure 12 shows that the damping ratio for the modes in between i and j will be smaller. For the modes higher than j the damping ratios will increase monotonically with frequency which means that the corresponding modal responses will be eliminated because of their high damping.

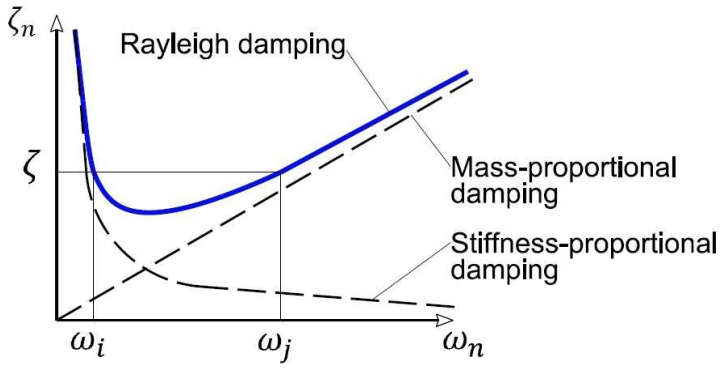

Figure 12 - Rayleigh damping

2.4.6 Lumped Mass

The mass matrix can be obtained using lumped mass instead of distributed mass throughout the structure. By applying statics the mass distribution of an element is equally assigned or lumped to its two nodes. This means that the lumped mass which has been assigned to a node is equal to sum of the mass contribution of all elements connected to that node. The lumped mass matrix is an idealization with satisfactory results where the mass matrix is diagonal because the rotational inertia has negligible influence on the dynamics of practical structures. Figure 13a shows the lumped mass of sample 2 where the mass matrix is expressed in 2.4.2. Figure 13b shows the assembling of relevant mass in the direction of DOFs.

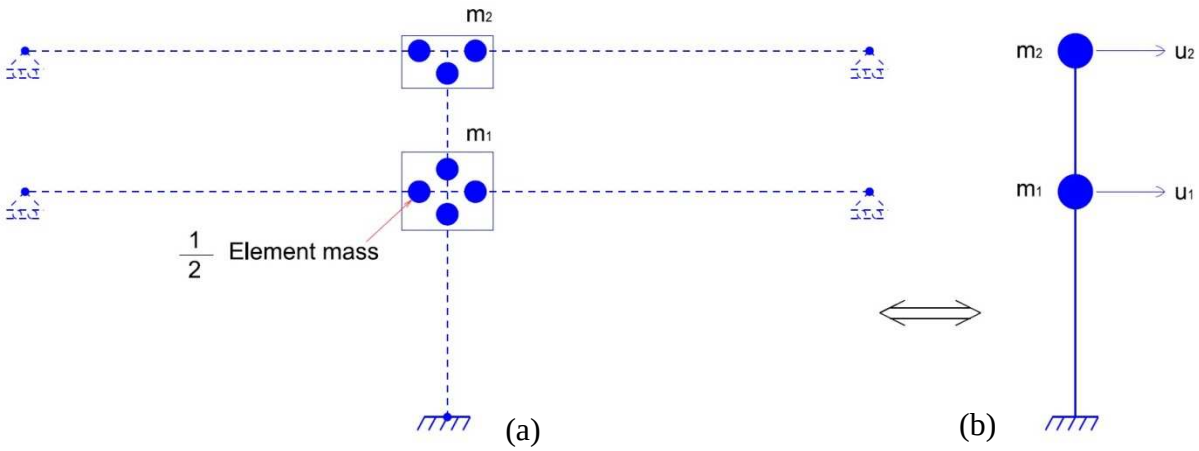

Figure 13 – (a) lumped mass for Sample 2, (b) simplified lumped mass

2.4.7 MDF Systems and Translational Ground Motion

The equation of motion for a MDOF system subjected to ground motion is:

$$[\boldsymbol{m}]\{\ddot{\boldsymbol{u}}(\boldsymbol{t})\} + [\boldsymbol{c}]\{\dot{\boldsymbol{u}}(\boldsymbol{t})\} + [\boldsymbol{k}]\{\boldsymbol{u}(\boldsymbol{t})\} = -\boldsymbol{m\iota}\ddot{u}_g(t) \qquad 2.4.6$$

Where vector $\boldsymbol{\iota}$ is the influence vector.

Figure 14 shows Sample 2 exposed to ground motion $\ddot{u}_g(t)$.

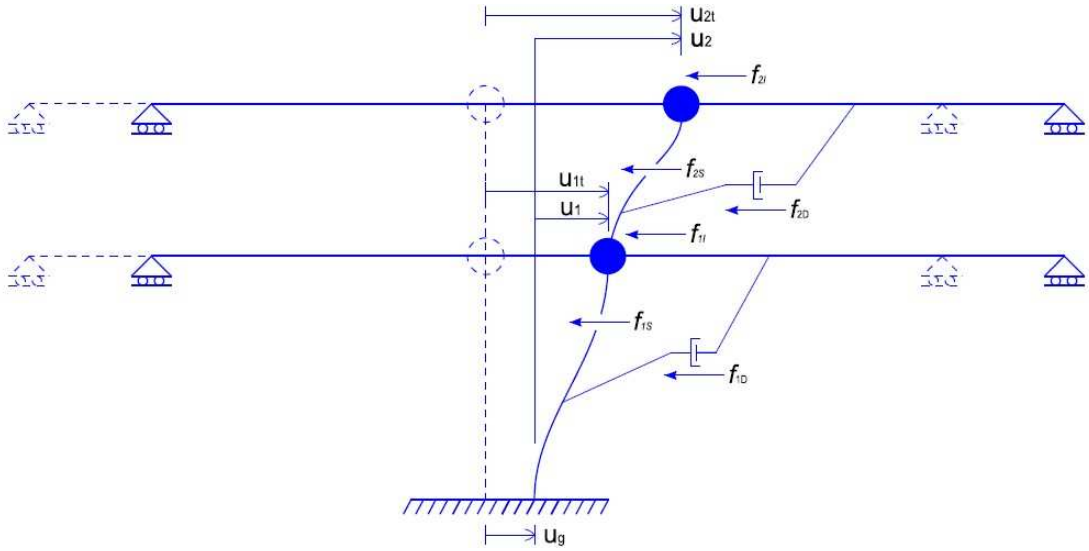

Figure 14 - Sample 2 exposed to ground motion

2.4.8 An Overview of Solution Methods for the Equation of Motion for a MDOF System

Methods for solving the equation of motion for a MDOF system can be divided in two categories.

I. Classical modal analysis: This method is appropriate for linear systems with classical damping. The solutions is in closed form for simple excitation and numerical for complex excitations. Modal analysis also stands as a ground base for response spectrum analysis. Both modal and response spectrum analysis are emphasized in this thesis and will be explained in detail in the following sections.

II. Direct analysis: This analysis method is suitable for both linear and nonlinear systems with classical or nonclassical damping. The solution is numerical.

2.4.9 Free Vibration for a MDOF System without damping

Equation of motion for a MDOF system without damping undergoing free vibration can be expressed as:

$$[\boldsymbol{m}]\{\ddot{\boldsymbol{u}}(\boldsymbol{t})\} + [\boldsymbol{k}]\{\boldsymbol{u}(\boldsymbol{t})\} = \{\boldsymbol{0}\} \qquad 2.4.8$$

It is necessary for a MDOF structure to undergo simple harmonic motion in order to determine its natural properties like the natural frequencies. One of the characteristics of a structure exposed to harmonic motion is its unchanged deflected shape which can be achieved if the free vibration is initiated by appropriate distribution of displacements in the various DOFs. Figure 15 shows two deflected shapes of Sample 2 while undergoing free harmonic vibration. Both superstructures pass through the equilibrium position and reach their extreme displacement at the same time. Each of these characteristic deflected shapes is called a natural mode of vibration for an MDOF system. As a rule of thumb; the number of modes of a structure is equal to the number of DOFs.

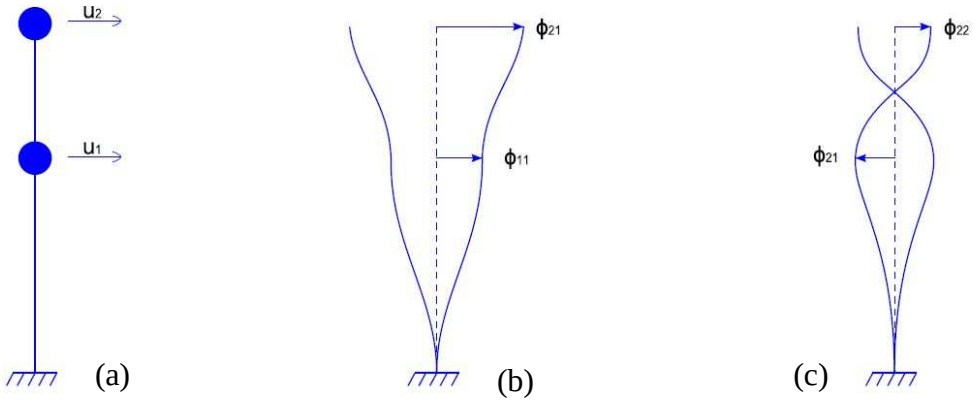

Figure 15 – (a) Simplified model of Sample 2, (b) mode shape 1, (c) mode shape 2

2.4.10 Eigenvalue problem for a MDOF System

The following equation shows how the displacement of an undamped system, sample 2 as an example, undergoing free vibration mathematically can be expanded:

$$\{\boldsymbol{u_n(t)}\} = \{\boldsymbol{\phi_n}\} q_n(t) \qquad 2.4.9$$

Were $\boldsymbol{u_n(t)}$ is the displacement vector for the nth mode, $\boldsymbol{\phi_n}$is the modeshape vector for the nth mode which do not vary with time and $q_n(t)$ denotes the modal coordinate which is time dependent. The time variation of the displacements is described by the simple harmonic function:

$$q_n(t) = A_n \cos(\omega_n t) + B_n \sin(\omega_n t) \qquad 2.4.10$$

Where A_n and B_n are integration constants that can be obtained from the initial conditions that initiated the motion.

By combining equations 2.4.9 and 2.4.10 and substituting these in 2.4.8 we can obtain the following algebraic equation which is called the eigenvalue problem:

$$\left[[\boldsymbol{k}] - {\omega_n}^{\boldsymbol{2}}[\boldsymbol{m}]\right]\{\boldsymbol{\phi_n}\} = \boldsymbol{0} \qquad 2.4.11$$

Where ω_n and $\boldsymbol{\phi_n}$ are unknown. The nontrivial solutions of 2.4.11 which means that when $\emptyset_{\boldsymbol{n}}$ is not equal to zero gives the natural frequency ω_n for the nth mode. And further 2.4.11 can be solved for $\boldsymbol{\phi_n}$ to within a multiplicative constant. The eigenvalue problem does not fix the absolute amplitude of the vector $\boldsymbol{\phi_n}$, only the shape of the vector given by the relative value of the nth displacements. This means that any vector proportional to $\boldsymbol{\phi_n}$ is essentially the same natural mode.

2.5 Modal Analysis

2.5.1 Introduction

As mentioned before, classical solution methods are not feasible for MDOF systems. The classical modal analysis offers a solution method for a linear MDOF system with classical damping excited by dynamic loading. The idea is to transform the equations of motion of a MDOF system to modal coordinates, leading to a set of uncoupled modal equations for a SDOF system which by solving gives the response contribution for every involved mode. This is also called the modal response. Further on, by combining these modal responses the total response can be obtained. An illustration of modal expansion is presented in figure 16 and in the following subsections this will be explained further.

2.5.2 Modal Equations for Undamped System Exposed to simple excitation

Equation of motion for a linear MDOF system without damping and exposed to harmonic dynamic excitation is expressed as:

$$[\boldsymbol{m}]\{\ddot{\boldsymbol{u}}\} + [\boldsymbol{k}]\{\boldsymbol{u}\} = \{\mathbf{p}(\boldsymbol{t})\} \qquad 2.5.1$$

The mathematical formulation for modal expansion of displacement was presented in section 2.4.10 and will be explained more detailed in the following. The total dynamic responses of a system which are expanded by modal coordinates can be expressed as:

$$\{\boldsymbol{u}(\boldsymbol{t})\} = \sum_{r=1}^{N} \{\boldsymbol{\phi_r}\}\, q_r(t) = [\boldsymbol{\Phi}]\{\boldsymbol{q}(\boldsymbol{t})\} \qquad 2.5.2$$

Where $\boldsymbol{u}(\boldsymbol{t})$ is the displacement vector, ϕ_r is the mode shape vector, $q_r(t)$ is scalar modal coordinate, $[\boldsymbol{\Phi}]$ is the modal matrix and $\boldsymbol{q}(\boldsymbol{t})$ is the modal coordinates vector.

By substituting 2.5.2 in 2.5.1, the following equation shows that 2.5.1 can be transformed to a set of uncoupled equations with modal coordinates as the unknown:

$$\sum_{\boldsymbol{r=1}}^{\boldsymbol{N}} [\boldsymbol{m}]\{\boldsymbol{\phi_r}\}\, \ddot{q}_r(t) + \sum_{\boldsymbol{r=1}}^{\boldsymbol{N}} [\boldsymbol{k}]\{\boldsymbol{\phi_r}\}\, q_r(t) = \{\mathbf{p}(\boldsymbol{t})\} \qquad 2.5.3$$

Premultiplying each term in 2.5.3 by ${\phi_n}^T$ gives:

$$\sum_{\boldsymbol{r=1}}^{\boldsymbol{N}} \{\boldsymbol{\phi_n}\}^{\boldsymbol{T}}[\boldsymbol{m}]\{\boldsymbol{\phi_r}\}\, \ddot{q}_r(t) + \sum_{\boldsymbol{r=1}}^{\boldsymbol{N}} \{\boldsymbol{\phi_n}\}^{\boldsymbol{T}}[\boldsymbol{k}]\{\boldsymbol{\phi_r}\}\, \boldsymbol{q_r}(\boldsymbol{t}) = \{\boldsymbol{\phi_n}\}^{\boldsymbol{T}}\{\mathbf{p}(\boldsymbol{t})\} \qquad 2.5.4$$

Orthogonality relations of modes, can show that all terms in each of the summations will be eliminated, except the $r = n$ term. By other means when $\omega_r \neq \omega_n$:

$$\{\boldsymbol{\phi_n}\}^{\boldsymbol{T}}[\boldsymbol{m}]\{\boldsymbol{\phi_n}\} = \mathbf{0} \qquad \{\boldsymbol{\phi_n}\}^{\boldsymbol{T}}[\boldsymbol{k}]\{\boldsymbol{\phi_n}\} = \mathbf{0} \qquad 2.5.5$$

And will results in the following reduced equation:

$$(\{\boldsymbol{\phi_n}\}^{\boldsymbol{T}}[\boldsymbol{m}]\{\boldsymbol{\phi_n}\})\ddot{q}_n(t) + (\{\boldsymbol{\phi_n}\}^{\boldsymbol{T}}[\boldsymbol{k}]\{\boldsymbol{\phi_n}\})q_n(t) = \{\boldsymbol{\phi_n}\}^{\boldsymbol{T}}\{\mathbf{p}(\boldsymbol{t})\} \quad \text{2.5.6}$$

2.5.6 can be expressed in generalized form as:

$$M_n\ddot{q}_n(t) + K_n q_n(t) = P_n(t) \quad \text{2.5.7}$$

Where

$$M_n = \{\boldsymbol{\phi_n}\}^{\boldsymbol{T}}[\boldsymbol{m}]\{\boldsymbol{\phi_n}\} \quad K_n = \{\boldsymbol{\phi_n}\}^{\boldsymbol{T}}[\boldsymbol{k}]\{\boldsymbol{\phi_n}\} \quad P_n(t) = \{\boldsymbol{\phi_n}\}^{\boldsymbol{T}}\{\mathbf{p}(\boldsymbol{t})\}$$

2.5.7 is the equation of motion for a SDOF system governing the response in modal coordinate $q_n(t)$ for the nth mode and therefore in scalar form. M_n is the generalized mass for the nth mode, K_n is the generalized stiffness for the nth mode $P_n(t)$ is the generalized force for the nth mode.

2.5.3 Modal Equations for Damped System Exposed to simple excitation

By the same method of section 2.5.2 the term for classical damping can be expanded to a set of uncoupled equations by modal coordinates. Thu, when damping is included in the modal equation it gives:

$$M_n\ddot{q}_n(t) + C_n\dot{q}_n(t) + K_n q_n(t) = P_n(t) \qquad 2.5.8$$

2.5.4 Toal Response

When the modal response, $q_n(t)$, is calculated either by 2.5.7 or 2.5.8 for $(n = 1, 2, \dots, N)$, the total response $\boldsymbol{u(t)}$ can then be obtained by combining the modal response for all the involved modes. This can be done by the following equation:

$$\{\boldsymbol{u(t)}\} = \sum_{n=1}^{N}\{\boldsymbol{u_n}(t)\} = \sum_{n=1}^{N}\{\boldsymbol{\phi_n}\}\, q_n(t) \qquad 2.5.9$$

2.5.5 Element Forces

The equivalent static force associated with the nth mode can be expressed as:

$$\{\boldsymbol{f_n(t)}\} = [\boldsymbol{k}]\{\boldsymbol{u_n(t)}\} \qquad 2.5.10$$

Substituting $\boldsymbol{u_n(t)} = \boldsymbol{\phi_n} q_n(t)$ in 2.5.10 gives:

$$\{\boldsymbol{f_n(t)}\} = \omega_n^2[\boldsymbol{m}]\{\boldsymbol{\phi_n}\}\ddot{q}_n(t) \qquad 2.5.11$$

Where $\boldsymbol{f_n(t)}$ is the nth mode contribution of an element force to the total force. And the total force is given by:

$$\{\boldsymbol{f(t)}\} = \sum_{n=1}^{N}\{\boldsymbol{f_n}(t)\} = \sum_{n=1}^{N}\omega_n^2[\boldsymbol{m}]\{\boldsymbol{\phi_n}\}\ddot{q}_n(t) \qquad 2.5.12$$

Where $\boldsymbol{f(t)}$ is the total element force.

2.5.6 Modal Expansion of Excitation Vector

The modal expansion of the excitation vector has useful properties as the force vector with its spatial distribution produces response only in the nth mode. Also the dynamic response in the nth mode is due entirely to the force vector contribution of the nth mode.

A harmonic excitation vector with its spatial distribution $\boldsymbol{s}$ is defined by:

$$\{\mathbf{p}(\boldsymbol{t})\} = \{\boldsymbol{s}\}p(t) \tag{2.5.13}$$

The aim of this section is to expand the vector $\boldsymbol{s}$ as:

$$\{\boldsymbol{s}\} = \sum_{\boldsymbol{r=1}}^{\boldsymbol{N}} \{\boldsymbol{s_r}\} = \sum_{\boldsymbol{r=1}}^{\boldsymbol{N}} \Gamma_r[\boldsymbol{m}]\{\boldsymbol{\phi_r}\} \tag{2.5.14}$$

As for the expansion of displacement vector, 2.5.15 can be obtained by premultiplying both sides of 2.5.14 by ${\phi_n}^T$ and the use of orthogonality relations for modes which gives:

$$\{\boldsymbol{s}\} = \sum_{\boldsymbol{n=1}}^{\boldsymbol{N}} \{\boldsymbol{s_n}\} = \sum_{\boldsymbol{n=1}}^{\boldsymbol{N}} \Gamma_n[\boldsymbol{m}]\{\boldsymbol{\phi_n}\} \tag{2.5.15}$$

Where $\boldsymbol{s_n}$ is the spatial contribution from the nth mode and is expressed as:

$$\{\boldsymbol{s_n}\} = \Gamma_n[\boldsymbol{m}]\{\boldsymbol{\phi_n}\} \tag{2.5.16}$$

Where

$$\Gamma_n = \frac{\{\boldsymbol{\phi_n}\}^T\{\boldsymbol{s}\}}{M_n} \tag{2.5.17}$$

Next it will be shown how the excitation vector with its spatial distribution can be adopted to the modal equation of 2.5.8. Dividing 2.5.8 by M_n gives:

$$\ddot{q}_n(t) + 2\zeta_n\omega_n\dot{q}_n(t) + \omega_n^2 q_n(t) = \frac{P_n(t)}{M_n} \qquad 2.5.18$$

As presented in 2.5.7 the generalized force $P_n(t)$ for the nth mode is $P_n(t) = \boldsymbol{\phi}_n^T\mathbf{p}(\boldsymbol{t})$ where $\mathbf{p}(\boldsymbol{t}) = \boldsymbol{s}p(t)$ and where $\boldsymbol{s} = \sum_{r=1}^{N} \Gamma_r \boldsymbol{m}\boldsymbol{\phi}_r$. These and the use of orthogonality relations of modes gives the following equation:

$$P_n(t) = \Gamma_n M_n\, p(t) \qquad 2.5.19$$

Substituting 2.5.19 in 2.5.18 gives:

$$\ddot{q}_n(t) + 2\zeta_n\omega_n\dot{q}_n(t) + \omega_n^2 q_n(t) = \Gamma_n P_n(t) \qquad 2.5.20$$

Equation 2.5.20 is the modal equation of motion for the nth mode subjected to a vector force with its spatial distribution. The factor Γ_n is called the participation factor which is an indication on whether enough modes are participating. Γ_n should be above 0.95 to get satisfactory results.

2.5.7 Modal Equations for Damped System Exposed to Ground Motion

The differential equation for a MDOF system exposed to earthquake induced ground motion is:

$$[\boldsymbol{m}]\{\ddot{\boldsymbol{u}}(\boldsymbol{t})\} + [\boldsymbol{c}]\{\dot{\boldsymbol{u}}(\boldsymbol{t})\} + [\boldsymbol{k}]\{\boldsymbol{u}(\boldsymbol{t})\} = -\boldsymbol{m\iota}\ddot{u}_g(t) \qquad 2.5.21$$

Where $\boldsymbol{\iota}$ is the influence vector which represents the unit displacement of the mass in the direction of the earthquake.

The modal expansion of displacement and forces are the same as presented in the previous sections with the exception of that the harmonic simple excitation will be replaced with the earthquake force as shown in the following equations.

The superposition of the modal contribution for a MDOF system is expressed in 2.5.9.

The spatial distribution of the earthquake force is defined by:

$$\boldsymbol{s} = \boldsymbol{m\iota} \tag{2.5.22}$$

As presented in section 2.5.6, we will expand the force distribution, in this case the earthquake force distribution, as a summation of modal inertia force distribution $\boldsymbol{s_n}$.

This gives:

$$\{\boldsymbol{s}\} = [\boldsymbol{m}]\{\boldsymbol{\iota}\} = \sum_{\boldsymbol{n=1}}^{\boldsymbol{N}} \{\boldsymbol{s_n}\} = \sum_{\boldsymbol{n=1}}^{\boldsymbol{N}} \Gamma_n [\boldsymbol{m}]\{\boldsymbol{\phi_n}\} \tag{2.5.23}$$

And by the use of orthogonality relations for modes the following can be obtained:

$$\Gamma_n = \frac{L_n}{M_n} \quad L_n = \{\boldsymbol{\phi_n}\}^T[\boldsymbol{m}]\{\boldsymbol{\iota}\} \quad M_n = \{\boldsymbol{\phi_n}\}^T[\boldsymbol{m}]\{\boldsymbol{\phi_n}\} \tag{2.5.24}$$

By repeating the same procedure for deriving 2.5.20 and the use of spatial distribution for earthquake force 2.5.23 and 2.5.24 instead of spatial distribution for $\mathbf{p}(\boldsymbol{t})$, we can drive the modal equation of motion for the nth mode subjected to earthquake induces ground motion.

$$\ddot{q}_n(t) + 2\zeta_n\omega_n\dot{q}_n(t) + \omega_n^2 q_n(t) = -\Gamma_n\ddot{u}_g(t) \tag{2.5.25}$$

Equation 2.5.25 can also be obtained by simply substitute the generalized force $P_n(t)$in 2.5.20 by the ground acceleration $\ddot{u}_g(t)$. Then 2.5.25 can be solved by a comparison approach to the equation of motion for a SDOF system to obtain the modal response for the nth mode. This is demonstrated next.

The equation of motion for a SDOF system exposed to ground motion is expressed as:

$$\ddot{u}_n(t) + 2\zeta_n\omega_n\dot{u}_n(t) + \omega_n^2 u_n(t) = -\ddot{u}_g(t) \tag{2.5.26}$$

By a quick comparison of 2.5.25 with 2.5.26 we can reveal the relation:

$$q_n(t) = \Gamma_n u_n(t) \tag{2.5.27}$$

By solving 2.5.26 by numerical time stepping methods for a SDOF system and using the relation 2.5.27, $q_n(t)$ in 2.5.25 can be obtained. Then the contribution of the nth mode to the nodal displacement can be expressed as:

$$\{\boldsymbol{u_n}(t)\} = \{\boldsymbol{\phi_n}\}q_n(t) = \Gamma_n\{\boldsymbol{\phi_n}\}u_n(t) \qquad \textbf{2.5.28}$$

The equivalent static element forces can be obtained by the following procedure. The equivalent static forces as presented in 2.5.10 is:

$$\{\boldsymbol{f_n}(\boldsymbol{t})\} = [\boldsymbol{k}]\{\boldsymbol{u_n}(\boldsymbol{t})\} \qquad \textbf{2.5.29}$$

By using 2.5.28, 2.5.29 can be rewritten as:

$$\{\boldsymbol{f_n}(\boldsymbol{t})\} = \omega_n^2[\boldsymbol{m}]\Gamma_n\{\boldsymbol{\phi_n}\}u_n(t) \qquad \textbf{2.5.30}$$

Where $[\boldsymbol{k}] = \omega_n^2[\boldsymbol{m}]$**.** Then by substituting 2.5.15 in 2.5.30 we can obtain the modal contribution of the nth mode to the total element force. :

$$\{\boldsymbol{f_n}(\boldsymbol{t})\} = \{\boldsymbol{s_n}\}A_n(t) \qquad \textbf{2.5.31}$$

Where $A_n(t) = \omega_n^2 u_n(t)$. The terms on the right side of 2.5.31 consists of the nth mode contribution $\boldsymbol{s_n}$ to the spatial distribution of the earthquake force and the pseudo acceleration response of the nth mode for a SDOF system to $\ddot{u}_g(t)$.

3 Earthquake

3.1 Introduction

In this section the most relevant aspects of earthquakes and sismology with respect to structural dynamics will be presented.

3.2 Seismology

Earthquakes are naturally broad-bended vibratory ground motions that occur due to tectonic ground motion, volcanism, landslide, man-made explosions and other actions with major effects on earth's crust. These ground motions can last from only a few seconds to several minutes. In most cases, shaking and ground failures are the dominant causes of damage. For this study we will only focus on natural earthquakes.

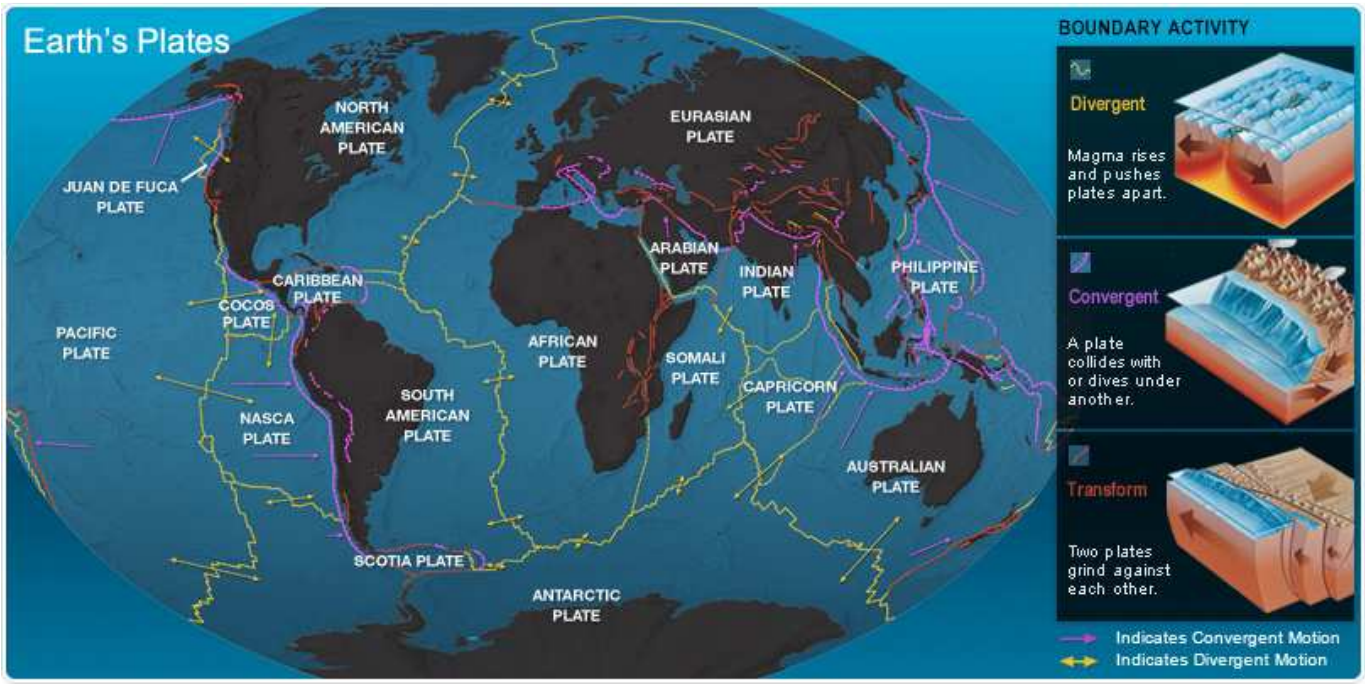

Figure 29 - Tectonic plates of planet earth

The vast majority of earthquakes originate in the vicinity of the boundary between crustal tectonic plates. The Earth's lithosphere consists of in total about 15 tectonic plates. These plates are driven by heat generated at the earth's core. Relative plate motion at the fault interface is constrained by friction. This accumulated energy in the plates will eventually overcome any resistance, and causes slip between the two sides of the fault.

This elastic rebound releases large amount of energy which initiates the earthquake. The first location of dynamic rapture is called the hypocenter, while epicenter is the projection on the surface of the earth directly above the hypocenter, see the figure 30.

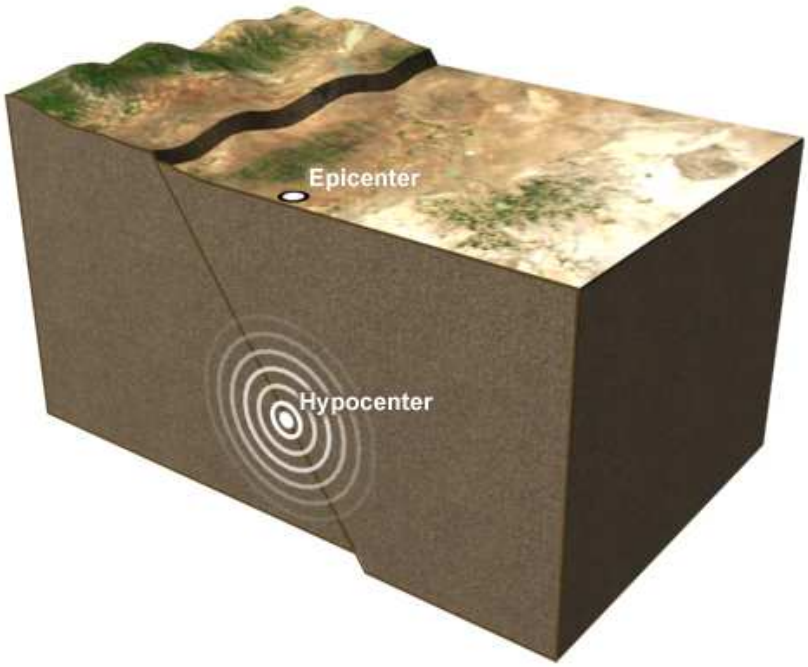

Figure 30 - An illustration of epicenter relative to hypocenter

The energy released by earthquakes is propagated over a broad spectrum of frequencies by different type of body and surface waves. Body waves which are originated at the rupture zone are classified as pressure waves P and shear waves S.

The faster P wave with particle movement parallel to the direction of the propagation, transmits energy via push and pull movements. The slower S waves with particle movement transverse to the propagation's direction, transmits shear action perpendicular to the motions direction. When body waves reach the ground surface some parts are reflected and other parts will generate surface waves. Surface waves are also classified in to two types of waves: Horizontally oscillating Love waves L, produces horizontal motion transverse to the direction of propagation, and vertically oscillating Rayleigh waves R produces a circular motion analogous to the motion of ocean waves.
S waves are generally the most important type of wave in term og earthquake resistant design since these are the waves that lead to most earthquake-related structural damage.

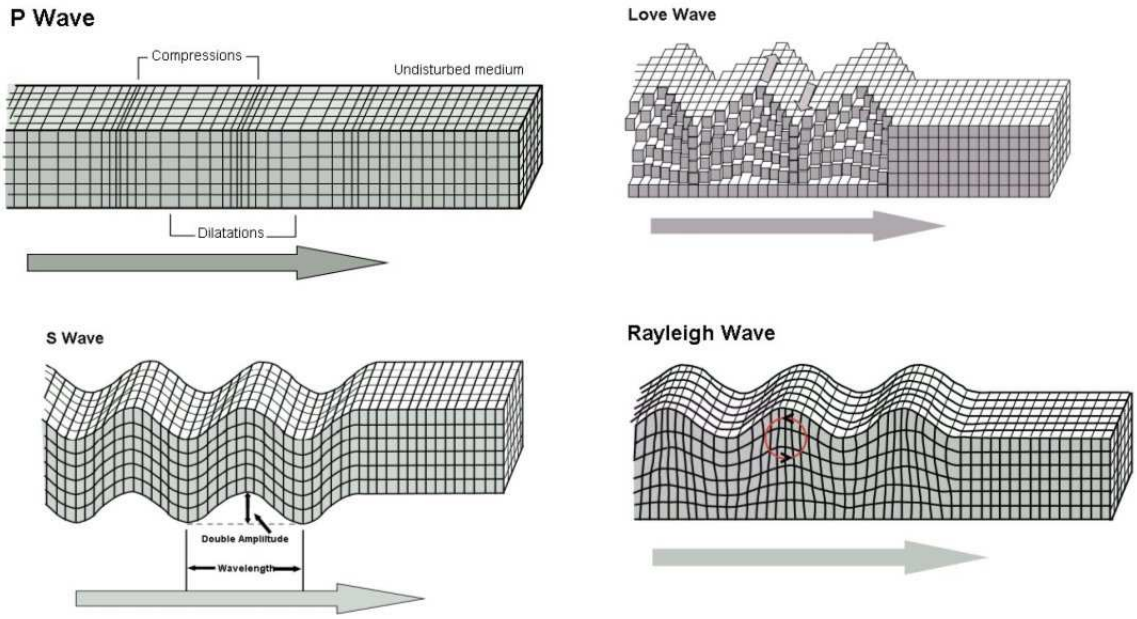

Figure 31 - Illustration of different wave form

Often, earthquakes are concentrated on faults. Faults that are moving more rapidly than others will tend to have higher rates of seismicity. Basic terms for classification of faults which is according to their sense of motion, includes:

- Strike slip
- Dip-slip
- Normal
- Reverse
- Thrust

3.3 Measurement of Earthquakes

The size of an earthquake is often measured in magnitude or intensity. The magnitude is the measure of the energy released at the source, while intensity is a measure of the effects of the ground motion at a given location.

Richter magnitude is a logarithmic scale and was developed to assign a single number to quantify the energy released during an earthquake.

The modified Mercalli scale quantifies the effects of an earthquake on the earth's surface, humans, objects of nature and manmade structures on a scale from I to XII, not felt to total destruction, respectively.

It has been shown that earthquakes with significantly different magnitude may induce similar intensities, depending on the location of the earthquake.

3.4 Seismometer

To record the motion of the earth during an earthquake, ground motion must be measured against something that remains relatively fixed. It means that it should not be affected by the shaking. In a seismometer, the fixed object consists of a mass suspended on springs within a case. During an earthquake, the mass remains still while the case around it moves with the ground shaking. Most modern seismometers work electromagnetically. A large permanent magnet is used for the mass and the outside case contains numerous windings of fine wire. Movements of the case relative to the magnet generate small electric signals in the wire coil.

Earthquake waves decrease in strength as they travel through the earth. High-frequency waves attenuate most severely; consequently, seismographs designed for monitoring local earthquakes must respond to a different frequency of ground motion from those used for recording distant earthquakes. Instruments sensitive to seismic waves that vibrate several times per second, called short period seismographs, are used to record local earthquakes, during which the waves reaching the seismograph are still very rapid and close together. Long period seismographs respond to lower frequency waves and are used to record distant events. Modern broadband seismographs perform both functions.

Some short period seismographs can magnify the ground motion several hundred thousand times. Such sensitive high-gain instruments can detect ground far movements too small to be felt by a human being. In the case of large earthquakes nearby, the ground motion may exceed the recording capacity of seismographs. To record the signals from large local earthquakes accurately, a third type of low-gain, Strong motion seismograph is needed. Strong motion seismographs apply minimal magnification (less than 100x), and are generally sensitive to ground acceleration.

Traditional strong motion instruments would not operate continuously, but only when triggered by strong ground movement, and would record only until the ground motion returned to an imperceptible level. Modern digital strong motion recorders are now replacing analog (photographic paper) recorders, and some have the option for continuous telemetry.

To completely characterize the earth's movement, the motion must be measured in three perpendicular directions. Consequently, seismographs often employ three sensors, recording in each of the north-south, east-west and vertical (up and down) directions.

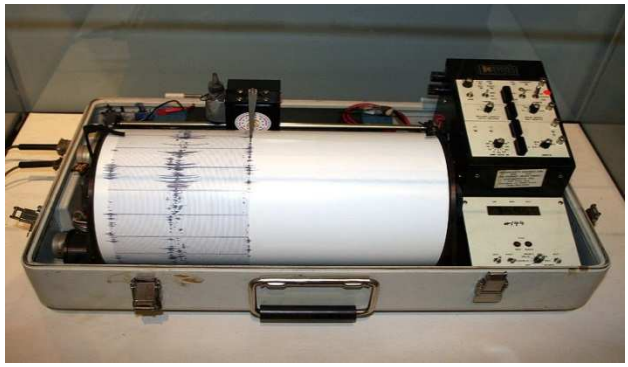

Figure 32 - Seismograph

4 Numerical modeling of two design options

4.1 Introduction

The numerical models have been established in two types of software: NovaFrame and OpenSees. Within a numerical model lies the mathematical formulation of geometry and material behavior of the bridge. There are several levels of discretization to be chosen from to describe a bridge's behavior under seismic loading. In this thesis, these two bridges are discretized to frame models consisting of linear elastic elements. The structural components are modeled using several elements, which are sufficient in number to describe the behavior of the bridge adequately.

4.2 Software Description

4.2.1 NovaFrame

NovaFrame is a space frame analysis program based on beam element theory. The program has a wide range of analysis capabilities, which in combination with a user friendly interface makes the program a versatile tool for a wide range of frame analysis tasks. The program is, in particular, well-suited for bridge structures but is just as suitable for basic analysis models.

4.2.2 OpenSees

OpenSees, the Open System for Earthquake Engineering Simulation, is an object-oriented, open source software framework. It allows users to create both serial and parallel finite element computer applications for simulating the response of structural and geotechnical systems subjected to earthquakes. OpenSees is primarily written in C++ and uses several Fortran and C numerical libraries for linear equation solving, and material and element routines.

4.3 Design Descriptions

The purposes of these two bridges are to carry traffic and pedestrians across the water safely. Both bridge designs follow the same vertical and horizontal road curvature and are combinations of two bridge types, a cantilever-bridge part and a beam-Bridge part with a variety of participation. The total bridge length is about 1200 meters horizontally and a maximum height of 35 meters above sea level. Reinforced concrete is used as building material. Sections between two towers are called main-span. Sections between a tower and a column are called main side-span. Sections between two columns are called side-span.

4.3.1 Cantilever Bridge

Figure 33 – A concrete cantilever bridge during construction

A concrete cantilever bridge is a type of bridge structure that uses the cantilever-beam principle as a construction method. In this case, big towers of concrete will ascend to the superstructures height where the construction of cantilever beams starts on each side of the tower horizontally into space without any supports except for the fixed points at the top of the tower. By casting the girder sections on each side of the tower almost simultaneously, the structure will manage to contain its balance before merging in to other structures or land. This bridge type is an effective structure for large spans up to 500 meters. The beam sections of a concrete cantilever bridge are usually casted as girders with varying section depth based on internal forces.

4.3.2 Beam Bridge

Figure 34 – A concrete beam bridge

A concrete beam bridge is the simplest structural form for a straight bridge span supported by columns and abutments. The columns are usually not fixed in to the beams and therefore no moment transfer will occur. The beam sections of a beam bridge in combination with a cantilever bridge are usually cast as a girder for the continuum of the superstructure as whole.

4.3.3 Bridge Design 1

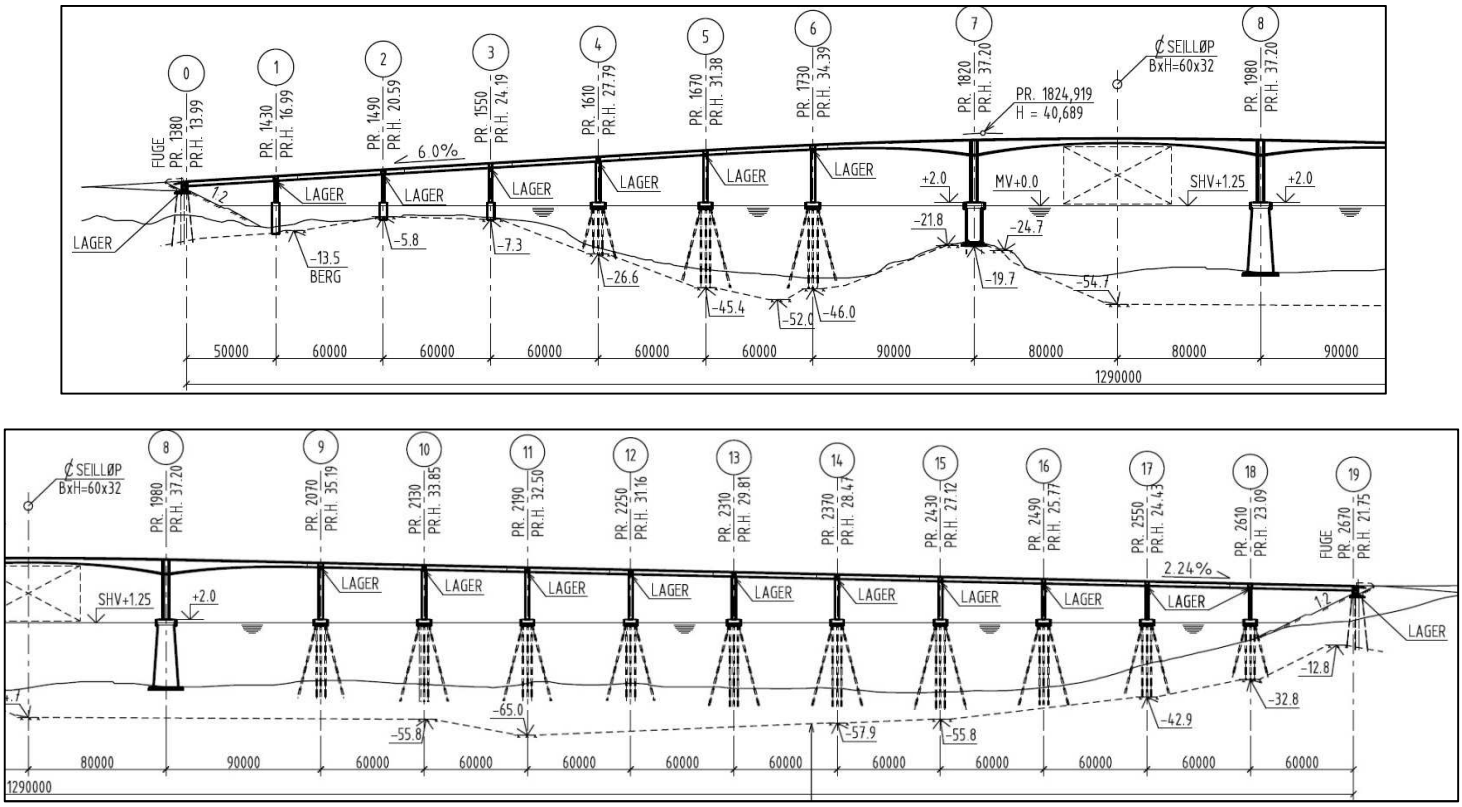

Figure 35 – Elevation of design 1 split in two with respect to visualization

Design 1 is mainly a beam bridge in combination with a Cantilever mid-section.

- Main span: 160 m supported by towers.
- Main side span 90 m supported by a tower and a column.
- Side spans 60 m supported by columns.
- Towers supported by subsea caissons.
- Columns supported by steel piles.

4.3.4 Bridge Design 2

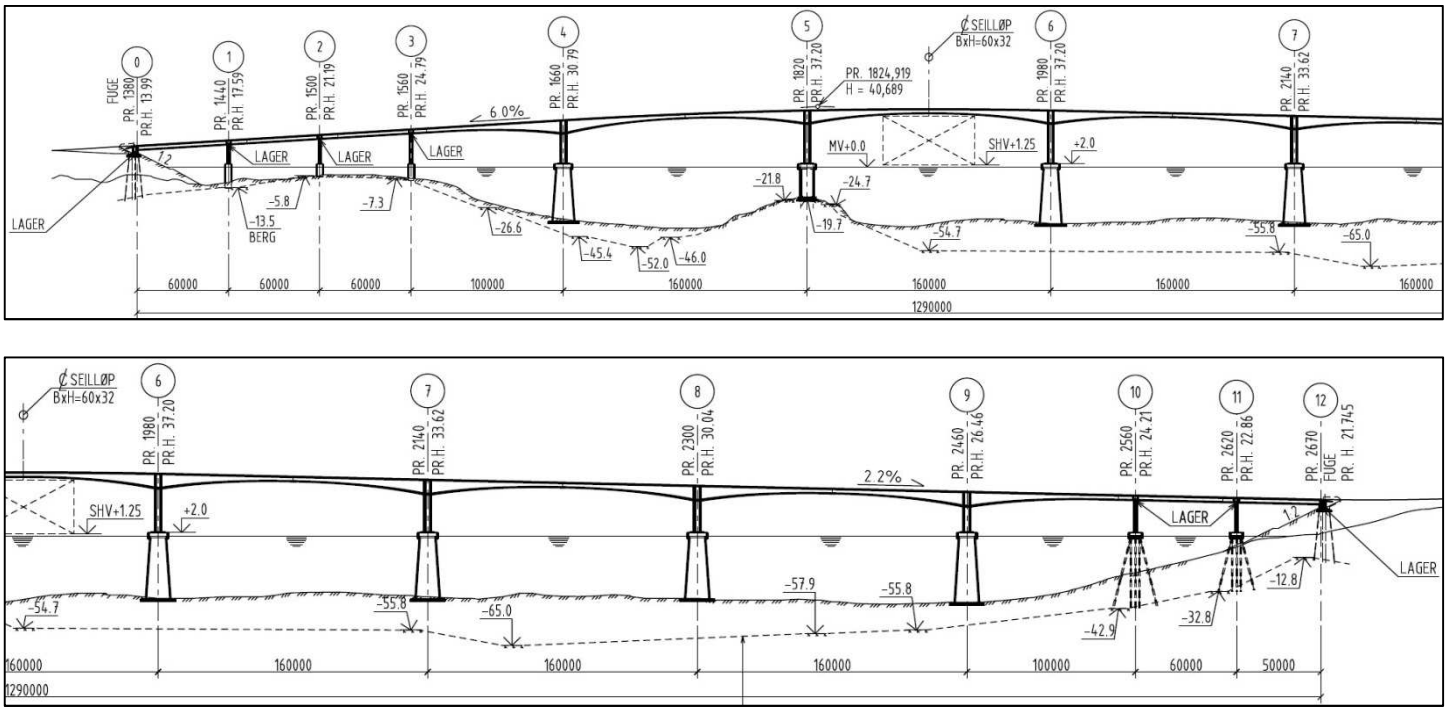

Figure 36 - Elevation of design 2 split in two with respect to visualization

Design 2 is mainly a cantilever bridge in combination with beam sections on both ends.

- Main span: 160 m supported by towers.
- Main side span 100 m supported by a tower and a column.
- Side spans 60 m supported by columns.
- Towers supported by subsea caissons
- Columns supported by steel piles

4.4 Modeling Assumptions and Limitations

Preparation of the numerical models of the two designs with the optimal representation of the reality is a time consuming process with need of a lot of accurate data at hand. For the purpose of this thesis which is mainly academic, the focus is on the analysis procedures and the comparison of two designs with respect to seismic loading. For this reason it is appropriate to make assumptions and idealizations to shorten the modeling process as much as possible without affecting the results with respect to the main focus.

4.4.1 Geotechnical Considerations

- Assumed on bed rock
- No soil-structure interaction

4.4.2 Concrete

Material properties

- Cylinder strength: $f_{ck} = 45$ MPa
- Young's modulus: $E = 36283$ MPa
- Poisson's ratio: $v = 0.2$

Design parameters

- ULS: 1.5
- ALS: 1.2

4.4.3 Reinforcement steel

Material properties

- Characteristic yield strength: $f_{yk} = 500$ MPa
- Young's modulus: $E_S = 200000$ MPa

Design parameters

- ULS: 1.15
- ALS: 1.0

4.4.4 Discretization

The numerical models in OpenSees and NovaFrame contain classic Bernoulli beam elements which represent all the bridge components. The discretization is much finer for the cantilever sections than the beam sections. This is done to catch the depth variation of the cantilever sections.

Design 1

The numerical model of design 1 consists of in total, 267 elements and 286 nodes. The structural components are discretized to the following number of elements and nodes:

- 26 elements and 27 nodes for the main-span. 1 main-span in total.
- 14 elements and 15 nodes per main-side-span. 2 main-side-spans in total.
- 5-6 elements and 6-7 nodes per ide-span. 16 side-spans in total.
- 6 elements and 7 nodes per column. 16 columns in total.
- 6 elements and 7 nodes per tower. 2 towers in total.
- 1 element and 2 nodes per tower-foundation. 2 tower-foundations in total.
- 5 elements and 6 nodes per caisson. 2 caissons in total.

Design 2

The numerical model of design 2 consists of in total, 291 elements and 303 nodes. The structural components are discretized to the following number of elements and nodes:

- 26 elements and 27 nodes per main-span. 5 main-spans in total.
- 15 elements and 16 nodes per main-side-span. 2 main-side-spans in total.
- 5-6 elements and 6-7 nodes per ide-span. 5 side-spans in total.
- 6 elements and 7 nodes per tower. 6 towers in total.
- 1 element and 2 nodes per tower-foundation. 6 tower-foundations in total.
- 5 elements and 6 nodes per caisson. 6 caissons in total.

4.4.5 Structural Mass

For the dynamic analysis, half of the element mass is concentrated at the closest node. This procedure is called the lump mass approach, which idealizes the mass distribution of an element as a concentrated mass at the element's end nodes. The mass of towers, piers and caissons are neglected in the longitudinal direction since these masses are insignificant compared to the mass of the superstructure.

4.4.6 Structural Damping

For the response spectrum analysis (RSA), an implicit damping ratio of ζ=5% has been used via a 5% damped response spectrum.

In the time history analysis (THA), 5% damping is defined using Rayleigh damping

4.4.7 Super Structure

As mentioned before, the superstructure of both bridges is a combination of a cantilever and beam bridges. The section height of the cantilever sections varies from 3 m up to 8.8 m while the height of the beam sections is 3 m constant as shown in figure. All the sections are casted as reinforced concrete girder. The girder is fixed to the top of the towers which means a full transfer of all forces in both directions. Between the column caps and the girder, gliding bearings are placed as isolation devices to contain displacements due to temperature deformations.

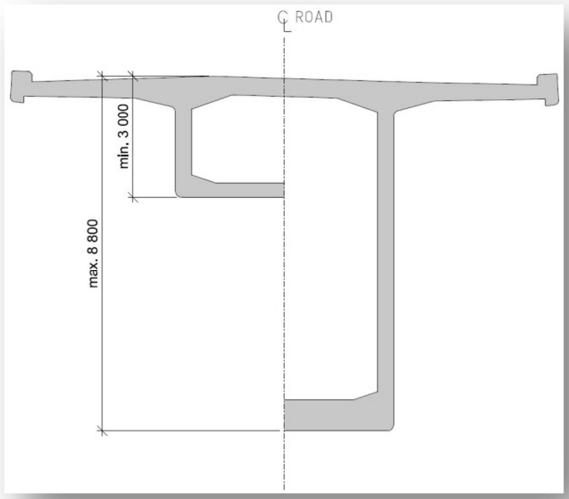

Figure 37 - Girder section

4.4.8 Tower

Towers are rectangular hollow concrete section consisting of thick walls with constant geometry at the entire height.

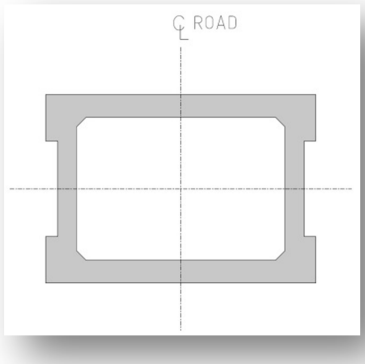

Figure 38 - Tower section

4.4.9 Column

Columns are rectangular concrete sections with constant geometry throughout the entire height. At the cap of each column two gliding bearing are placed due to displacement caused by temperature. The maximum displacements of these bearings are limited by utilizing the friction force due to dead weight of the superstructure. The bases of the columns are assumed to be fixed at water level. Due to the isolation devices there will be no transfer of moments and shear forces between columns and the superstructure. Thus, no additional shear forces and moments are transferred to the columns.

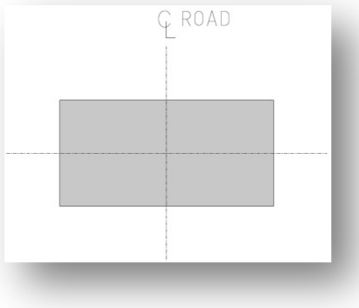

Figure 39 - Column section

4.4.10 Tower Foundation

Tower foundations are circular concrete sections with constant geometry at the entire height. These are the connecting point between towers and caissons.

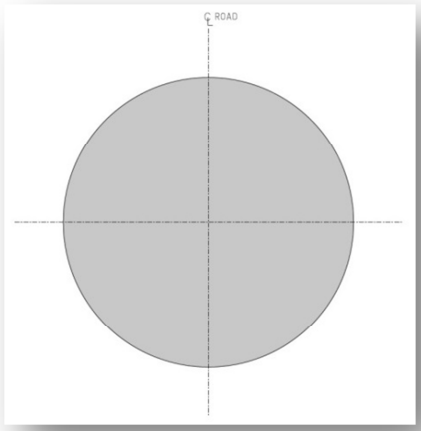

Figure 40 - Tower foundation section

4.4.11 Subsea Caisson

Caissons are modeled as circular hollow concrete section with thick walls and constant geometry at the entire height. When the caissons are submerged they will be filled with gravel which will contribute to the overall stiffness. For this thesis the stiffness contribution from the gravel mass is neglected and instead caissons wall thicknesses are being edited to compensate for this loss of stiffness. The bases of all caissons are resting on the bed rock and are modeled as fixed supports in all directions.

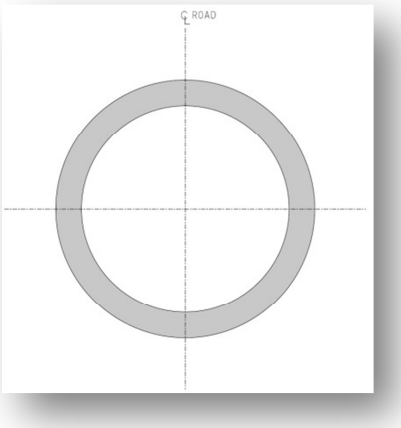

Figure 41 - Caisson section

4.4.12 Abutment

Like the columns the abutments also do note contribute to the resisting force against seismic loading. Thus the abutments are modeled as simply supported points which are fixed only in vertical direction.

4.4.13 Loads

Only two types of loads are considered for the purpose of the analysis:

- Dead weight of the reinforced concrete equivalent to $25\,\frac{kN}{m^3}$
- Seismic loading from 7 different ground motions.

5 Numerical Analysis and Discussion of Results (longitudinal)

5.1 Introduction

2D models summarized in the previous section were analyzed in both NovaFrame and OpenSees using different methods and the results were evaluated. NovaFrame uses the response spectrum analysis (RSA) as main method for dynamic analysis while OpenSees is specialized in time history analysis (THA). By using different methods of analysis we will have a reliable foundation for comparison of these methods and the designs.

Figure 43 and 44 shows the order spans and columns are named in for both designs. The figures also show specified sections, that is tower caps, tower bases and caisson bases. These are sections where forces and displacements are to be analyzed both in longitudinal (chapter 5) and transverse (chapter 6) direction.

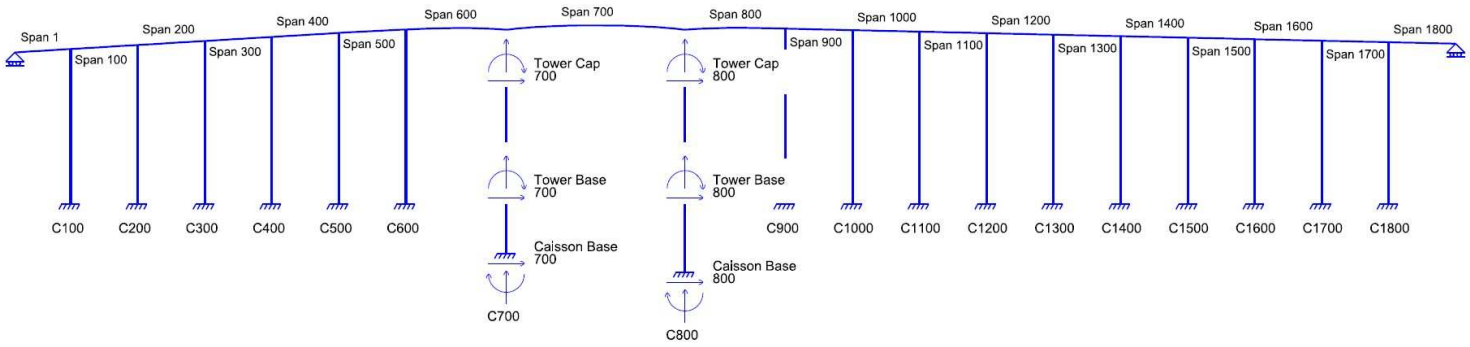

Figure 42 - Numerical model notations for design 1

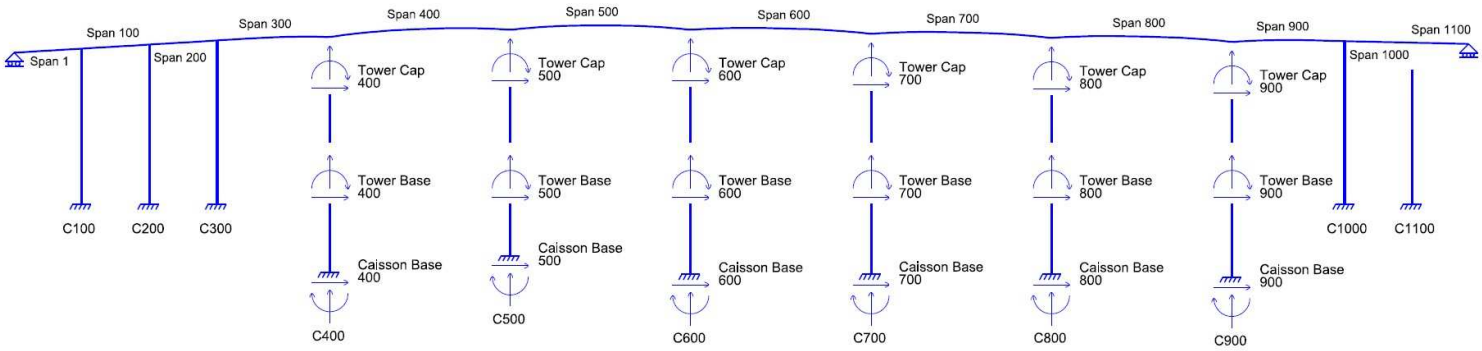

Figure 43 - Numerical model notations for design 2

The Chapter starts by solving the eigenvalue problem for the two designs in both software. Then the response spectrum (RS) for selected ground motions will be obtained and scaled with respect to design spectrum (DS) which also will be obtained by following the guide lines of the Eurocode 8. NovaFrame will then use these scaled response spectrums to run a RSA for both designs. Furthermore, OpenSees will run a THA for each ground motion for the two designs.

In general, seismic design will always try to avoid shear damage while damage in the form of flexural yielding is allowed to occur in columns. Assuming this, only flexural forces will be evaluated. And since this thesis is limited to horizontal ground motion, we will only be interested in horizontal displacement, which is accepted as an indication of earthquake related damage.

5.2 Eigenvalue Analysis (EVA) in Longitudinal Direction

The EVA is the first and an important step for identifying the natural properties of both designs.

By solving the eigenvalue problem and comparing the results for the two designs we will also get a god confirmation on how accurate the numerical models are compared to each other and whether the models can be used for further comparisons.

5.2.1 Results of Eigenvalue Analysis (EVA) in Longitudinal Direction

The eigenvalues connected to the ten first mode shapes in the longitudinal direction of both design are obtained in NovaFrame and OpenSees by EVA where the results are presented in table 1 and 2. For civil engineering purposes it is very common to express the Eigen modes in term of natural cyclic frequency or natural period. These first modes are especially valuable when later we will use these to define spectral points in NovaFrame. The first three natural mode shapes are illustrated for each design in fig. 45 and 46 below.

Table 1 - Natural frequency and the modal mass participation of design 1, longitudinal

Design 1			**Novaframe**	**Opensees**	
	Modal participation	Natural cyclic frequency	Natural period	Natural period	Natural cyclic frequency
	%	f, Hz	T, s	T, s	f, Hz
Mode 1	0.996	0.487	2.05	2.05	0.487
Mode 2	0.003	1.499	0.67	0.67	1.498
Mode 3	0.001	2.897	0.35	0.35	2.896
Mode 4	0.00	4.325	0.23	0.23	4.325
Mode 5	0.00	5.691	0.18	0.18	5.690
Mode 6	0.00	7.307	0.14	0.14	7.305
Mode 7	0.00	8.299	0.12	0.12	8.296
Mode 8	0.00	10.169	0.10	0.10	10.167
Mode 9	0.00	11.424	0.09	0.09	11.417
Mode 10	0.00	12.778	0.08	0.08	12.774

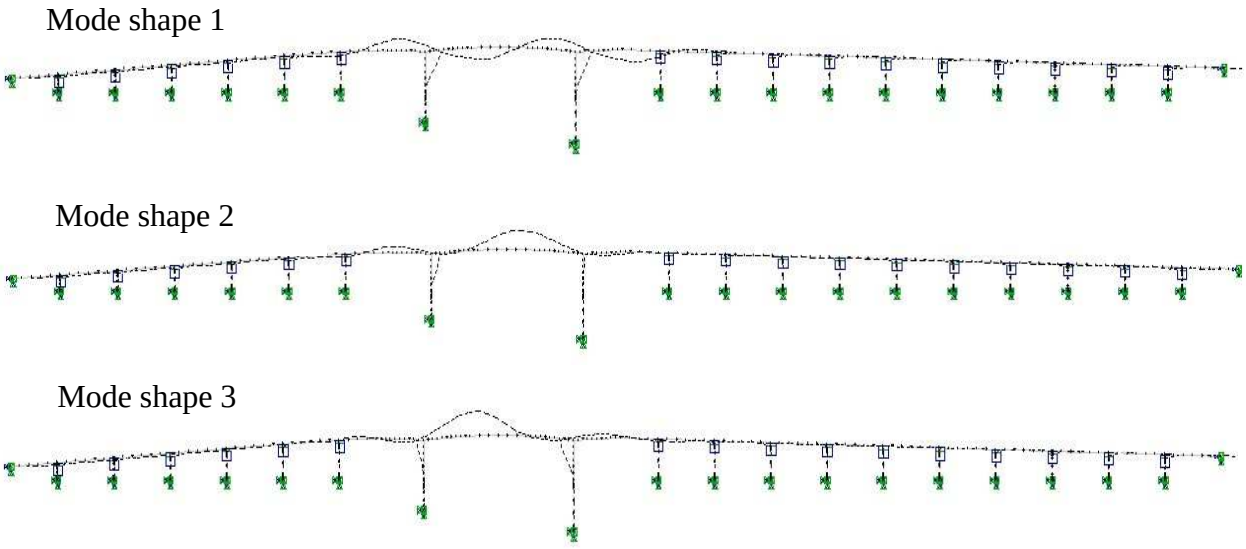

Figure 44, mode shape 1, 2 and 3 of design 1, longitudinal

Table 2, Natural frequency and the modal mass participation of design 2, longitudinal

Design 2			Novaframe	Opensees	
	Modal participation	Natural cyclic frequency	Natural period	Natural period	Natural cyclic frequency
	%	f, Hz	T, s	T, s	f, Hz
Mode 1	0.985	0.953	1.05	1.02	0.983
Mode 2	0.014	1.682	0.59	0.58	1.732
Mode 3	0.00	2.876	0.35	0.34	2.965
Mode 4	0.00	4.152	0.24	0.23	4.282
Mode 5	0.00	5.408	0.18	0.18	5.578
Mode 6	0.00	6.671	0.15	0.15	6.881
Mode 7	0.00	7.506	0.13	0.13	7.742
Mode 8	0.00	8.931	0.11	0.11	9.214
Mode 9	0.00	10.814	0.09	0.09	11.141
Mode 10	0.00	11.982	0.08	0.08	12.350

Mode shape 1

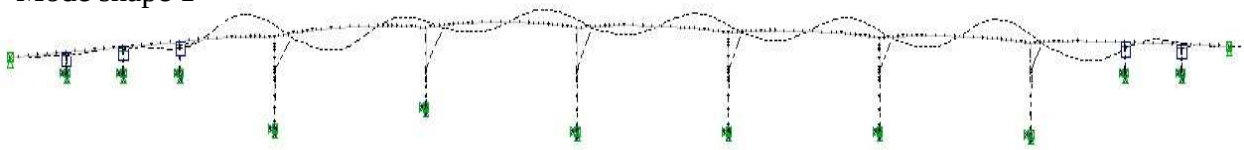

Mode shape

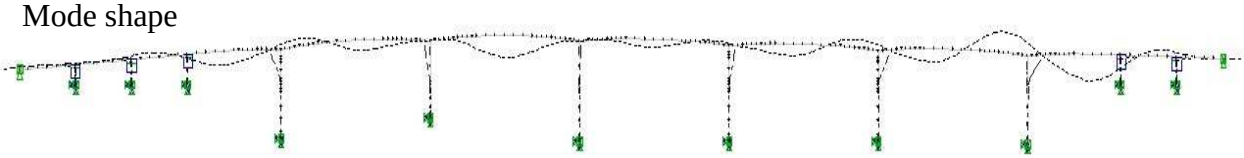

Mode shape 3

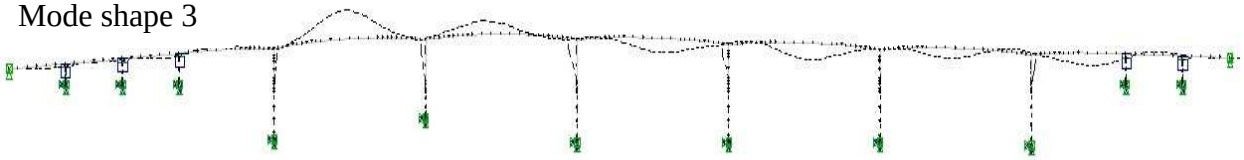

Figure 45, mode shape 1, 2 and 3 of design 2, longitudinal

5.2.2 Discussion of Results (EVA), Longitudinal

From table 1 and 2 it can be seen that the natural properties of each design computed in NovaFrame and OpenSees corresponds perfectly. These results confirm that the numerical models established in both software are good basis for further comparison.

When it comes to the comparison of the two designs we can observe that the first periods of design 1 are much larger than design 2. As observed, the duration of each cycle in the first mode for design 1 is 2.05 seconds while the second design uses only 1.05 second. This indicates that design 1 is a much more flexible structure and hence it uses more time to go through one complete oscillation. This observation complies very much with the reality when we know that the longitudinal resistance for design 1 against ground motion comes mostly from two towers, while design 2 has six towers with contribution to the same longitudinal resistance.

5.3 Elastic Response Spectrum Analysis (RSA) in Longitudinal Direction

Structural design is mostly based on the peak responses of the structure during the duration of an earthquake induced ground motion. For a civil engineer, RSA is an efficient analysis procedure with the use of peak responses without consuming too much time. In this section several earthquakes will be selected and by using OpenSees and Matlab codes, the response spectra for each earthquake will be generated. The response spectra will then be scaled to the level of the design spectrum specified by Eurocode with respect to seismic zones. Furthermore, the peak modal responses in term of pseudo-acceleration and frequency for the two designs ten first natural modes under each ground motion will be retrieved from the scaled response spectra. These ten selected response quantities from each scaled response spectra will be used as spectral points in NovaFrame. Based on this information NovaFrame will be able to calculate all responses of the two bridge designs.

5.3.1 Ground Motion (Unscaled)

To be able to evaluate the response behavior of these two bridge designs clearly, seven different horizontal ground motions that were recorded in the west coast of U.S. by seven different monitoring stations are selected. These selections are based on the representative soil type in the area and the soil's shear wave velocity. These ground motions varies in magnitude, distance from fault, type of fault, geology of the traveling distance and duration, to an extent. The relevant information is shown in table 3. Acceleration time history of all ground motion records are plotted in figure 37.

Table 3 - Ground motion information

Comp.	NGA#	Event	Year	Station	Mag	Mechanism	Vs30(m/s)
GM	149	Coyote Lake	1979	Gilroy Array #4	5.7	Strike-Slip	221.8
GM	1990	Gulf of California	2001	Bonds Corner	5.7	Strike-Slip	223.0
GM	193	Imperial Valley-07	1979	Bonds Corner	5.0	Strike-Slip	223.0
GM	1701	Northridge-06	1994	Hollywood - Willoughby Ave	5.3	Reverse	234.9
GM	314	Westmorland	1981	Brawley Airport	5.9	Strike-Slip	208.7
GM	608	Whittier Narrows-01	1987	Carson - Water St	6.0	Reverse-Oblique	160.6
GM	1844	Yountville	2000	Alameda - Oakland Airport FS #4	5.0	Strike-Slip	202.4

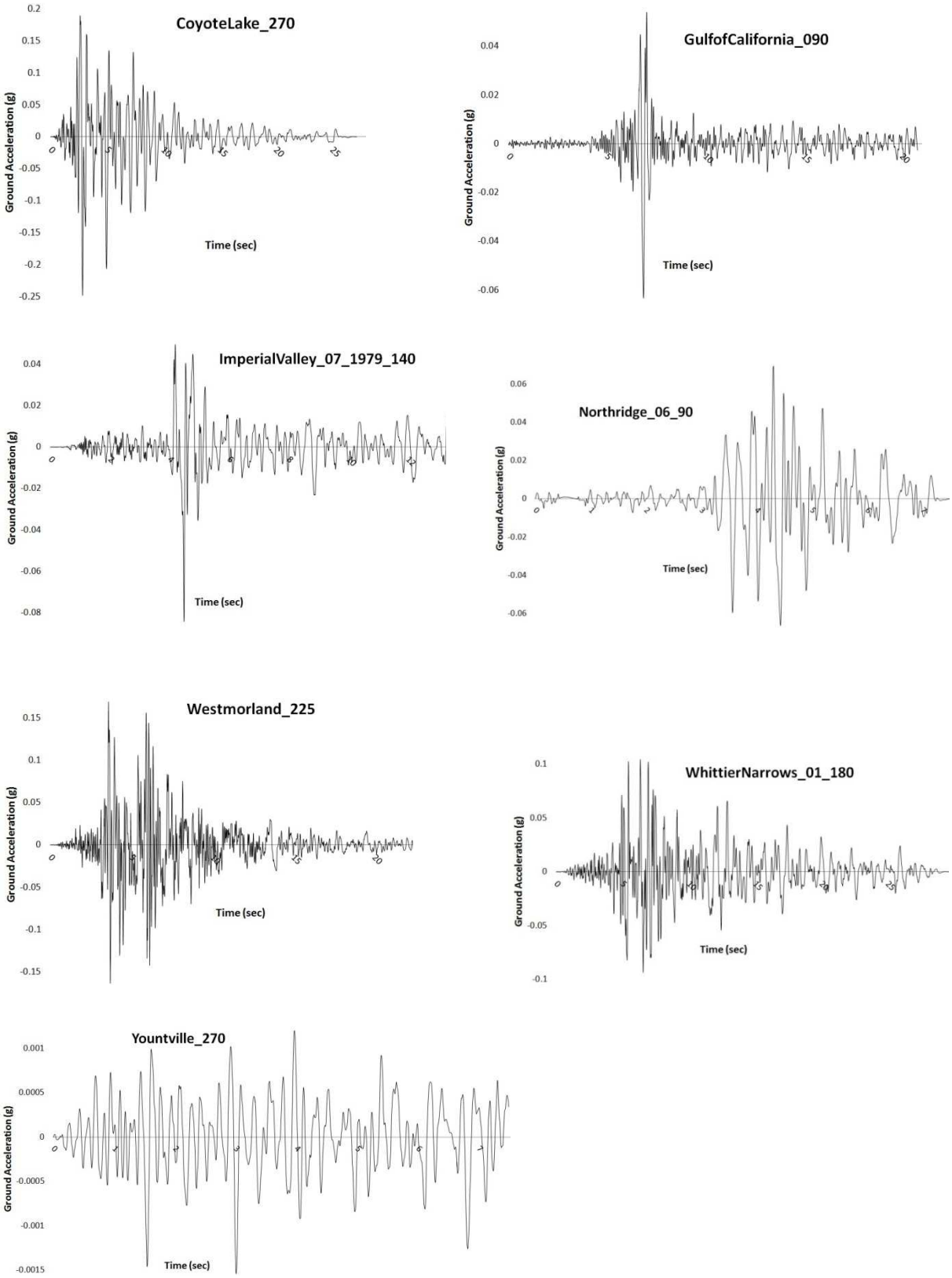

Figure 46 - ground motion recordings for seven earthquakes from California

5.3.2 Construction of Response Spectrum (RS)

A two-node SDOF system with zero element length, a single mass unit and a unit of section area is modeled in OpenSees. Then one of the selected ground motions is applied to the system as a seismic loading using several time steps with a constant time step increment. OpenSees runs several loops of dynamic analysis for a set of periods where the deflection of the single mass in term of horizontal deformation can be obtained for each period. The peak deformation of the mass for each period is assembled with help of Matlab to a displacement RS. Furthermore, the pseudo-acceleration response spectrum can be calculated directly from the displacement RS by using the relationship, $A = \omega_n^2 D$. This procedure has been done for all seven earthquakes and the pseudo-acceleration response spectrum has been generated for every one of them. Figure 48 and 49 shows the Matlab plot of pseudo-acceleration RS for two of the ground motions.

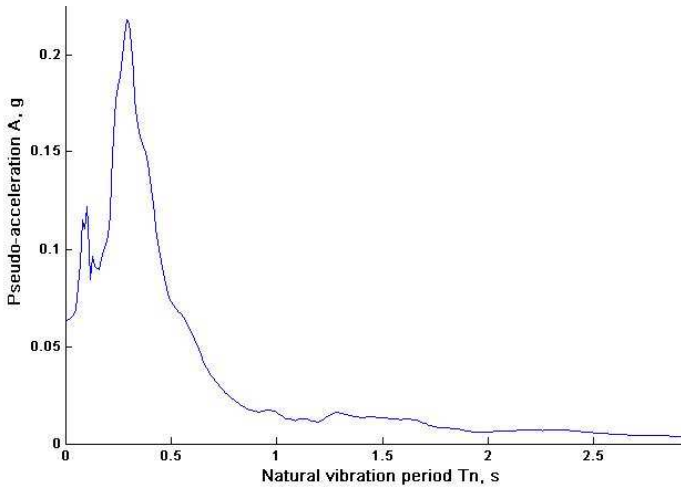

Figure 47, RS Gulf of California

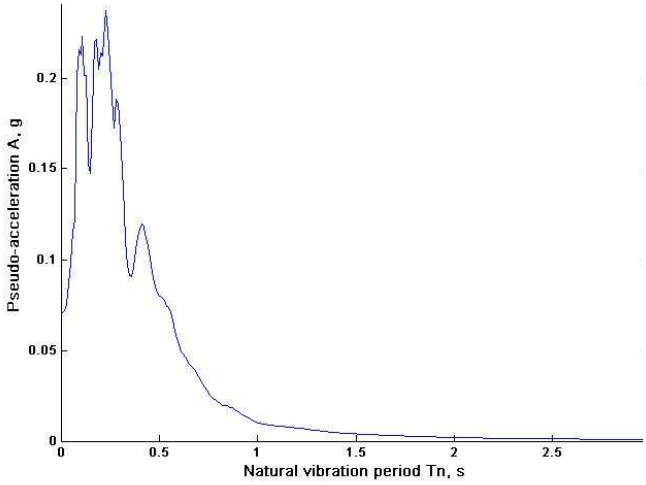

Figure 48, RS Northridge

5.3.3 Obtaining Design Spectrum (DS) According to Eurocode 8

According to the Eurocode 8, EC 8-2 NA.2.1, a bridge with a total length $L_{tot} > 600m$ is classified as importance class IV and the associated importance factor $\gamma_I = 2.0$. The reference return period $T_{NCR} = 475$ years; this corresponds to $P_{NCR} = 50$ years which is the probability of exceedance of 10% in 50 years.

The overall representation of the soil type is determined as soil type E by testing soil samples. The soil factor of elastic spectrum is $S = 1.7$ and the behavior factor is set to $q = 1.5$. From EC 8-1 table NA.3.3 and figure NA.3 the following parameters are retrieved: $T_B = 0.1,\ T_C = 0.35,\ T_D = 1.5,\ a_{g40Hz} = 0.7.$

The design ground acceleration can then be computed as:

$$a_g = \gamma_I a_{gR} = \gamma_I 0.8 a_{g40Hz} = 0.114169g$$

Based on the information above the following design spectrum in figure 50 is constructed:

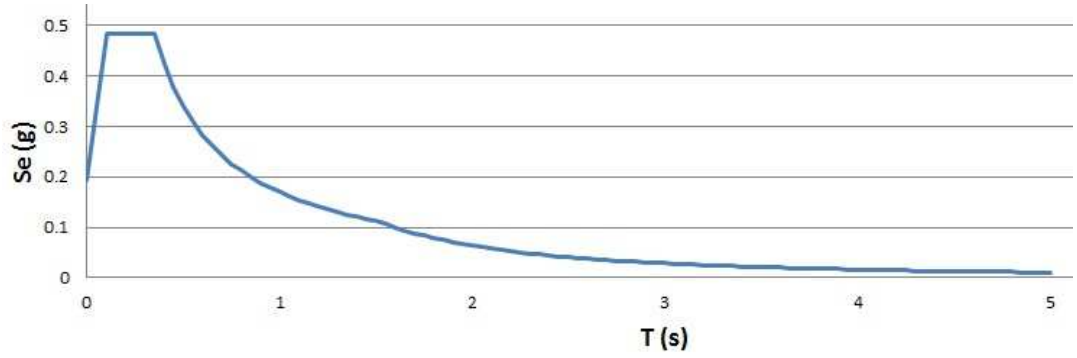

Figure 49 - Horizontal elastic design spectrum

5.3.4 Scaled Ground Motion in Longitudinal Direction

As it turned out, collecting ground motion data from Norway was not an easy task. And therefore, the selected ground motions are originated from California which is a high seismicity region. In order for these ground motions to be representative for Norway and never the less the location of the bridge which is a low seismicity region we need to scale their response spectrums which were generated in section 6.3.2. This is done by scaling the response spectrums with respect to the first mode for each design. This means that the spectral acceleration of every response spectrum for the first period has to coincide with the design spectrum. Table 4 shows the scale factor of every ground motion for both designs. S_e denotes the spectral acceleration of RS or DS in units of g.

Table 4 – Spectral acceleration for the response and design spectra measured in g and scaling factor values for longitudinal direction

		Design 1			Design 2		
EQ. No.	T_mode 1 EarthQuake name	S_e RS	S_e DS	2.05 Scaling Factor	S_e RS	S_e DS	1.05 Scaling Factor
1	Coyote Lake	0.0628	0.0606	0.966	0.2643	0.1617	0.612
2	Gulf of California	0.0064	0.0606	9.495	0.0128	0.1617	12.646
3	Imperial Valley-07 1979	0.0034	0.0606	18.084	0.0240	0.1617	6.739
4	Northridge-06	0.0019	0.0606	32.072	0.0090	0.1617	18.065
5	Westmorland	0.0885	0.0606	0.685	0.0963	0.1617	1.680
6	Whittier Narrows-01	0.0226	0.0606	2.687	0.0988	0.1617	1.638
7	Yountville	0.0020	0.0606	30.491	0.0059	0.1617	27.376

The plot of scaled response spectrums of the seven ground motions for bridge design 1 and 2 along with the design spectrum from section 6.3.3 is shown in Figure 51 and 52, respectively. In figure 51 we can observe that all the scaled spectrums of design 1 coincide with the design spectrum for $T = 2.05$s. In the same way we can observe coincided scaled spectrums for design 2 along with the design spectrum for $T = 1.05$s in figure 52.

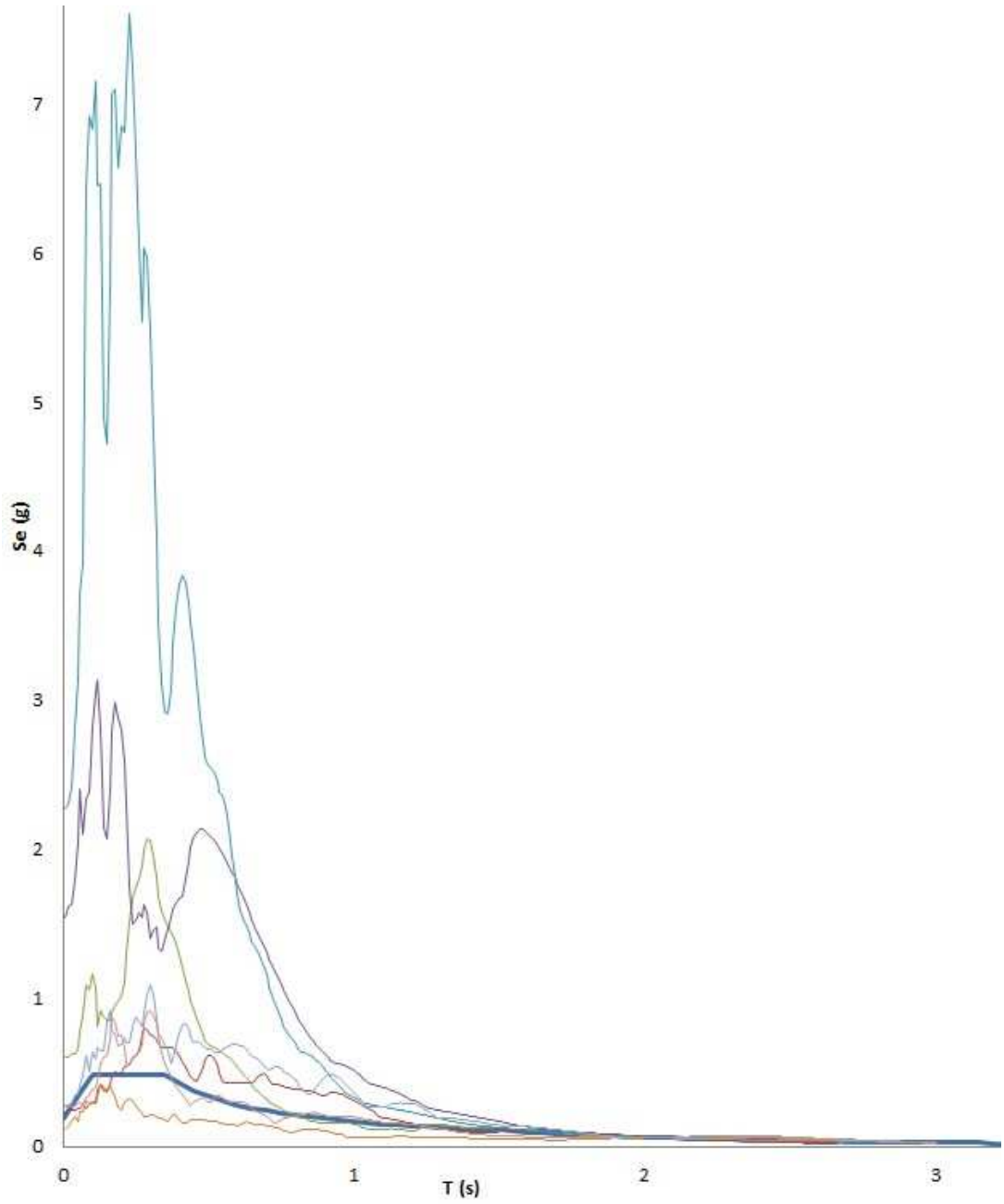

Figure 50 - Scaled spectral acceleration for design 1 in longitudinal direction

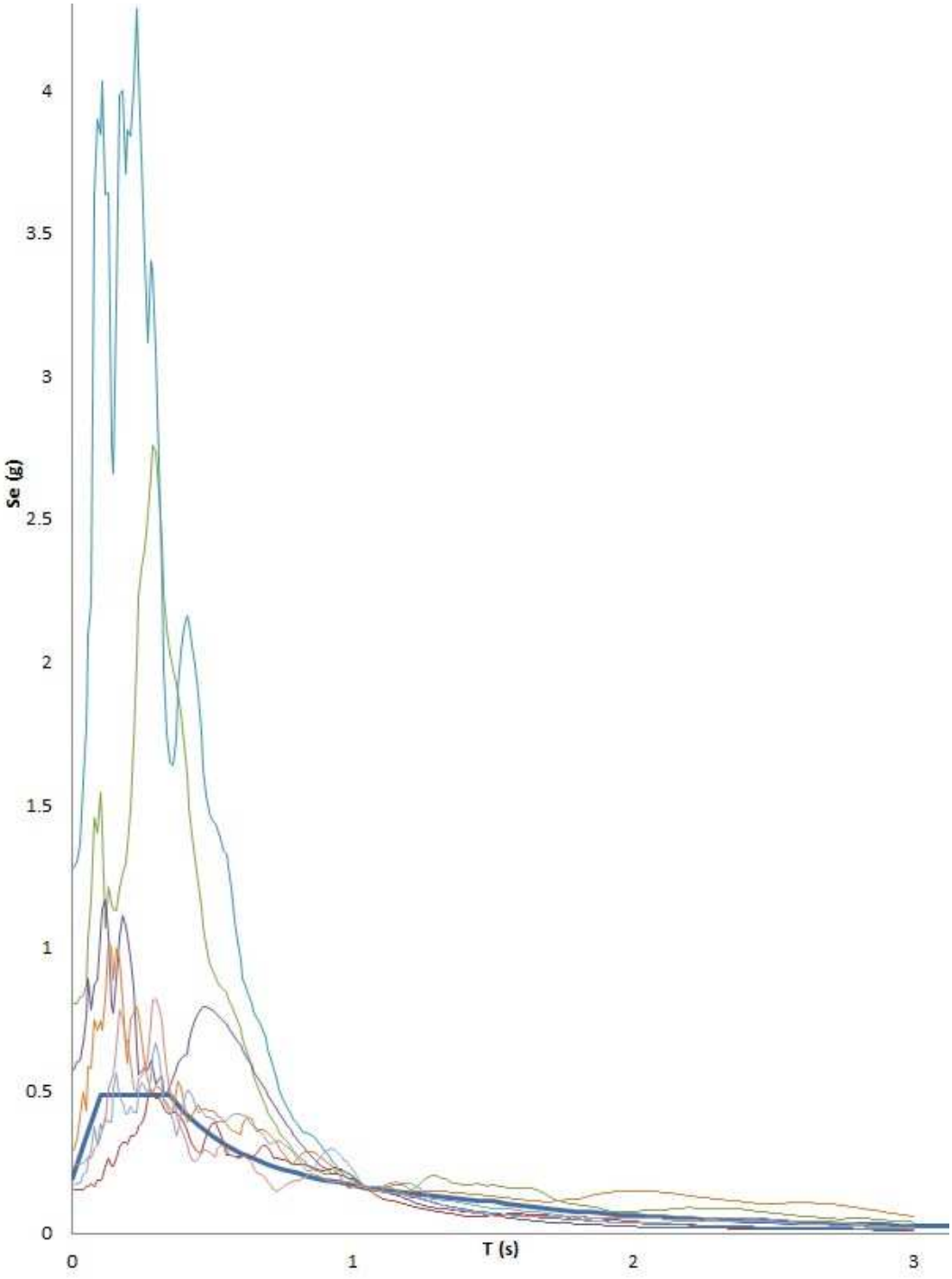

Figure 51 - Scaled spectral acceleration for design 2 in longitudinal direction

We have now obtained representable spectral accelerations and can go on to start the RSA by NovaFrame.

5.3.5 RSA in NovaFrame

The dynamic analysis in NovaFrame is based on modal calculations. The RSA method for a MDOF system is the only approach this software offers. By using modal analysis it calculates the static responses for each mode in term of deflections and section forces. Then it multiplies each modes deflection with the values obtained from the response spectra to calculate the peak modal response. Furthermore, NovaFrame uses the Root-Mean-Square as combination rule to obtain the total structural response. This combination rule is not valid for closely spaced modes, that is, closely spaced natural frequencies. It only offers the possibility to inspect the results for closely spaced modes in order to determine whether other types of combination rules are required. In order to determine number of sufficient modes for the modal calculation NovaFrame calculates the participation factor which is obtained from normalized modal mass ratio.

Although NovaFrame has predefined response spectrum defined by Seismic Zonation of Norway, for this thesis it is chosen to employ user defined response spectrum for two reasons. The first reason is to use this opportunity to learn the whole developing process of a response spectrum and make use of it. Secondly the two bridge designs will be analyzed for the same ground motions both in the RSA and THA, and comparison of these designs will be possible.

NovaFrame does not allow importing of a response spectrum as a whole. As mentioned in section 6.2.1 the obtained natural frequencies in table 1 and 2 and their related scaled spectral accelerations for each ground motion are used as spectral points as input in NovaFrame. This is basically a simplified method for importing a response spectrum where NovaFrame generates smooth lines by interpolations. Since RSA is a method based on modal analysis it is appropriate to choose the spectral points with respect to the designs natural periods as NovaFrame retrieves the exact same points to do the analysis. And later we will see that three spectral points are enough to do the analysis in the longitudinal direction since the mode participation factors shows the need of only three modes for engaging all the mass.

5.3.6 Results and Discussion of RSA in Longitudinal Direction

Design 1 and Design 2 are exposed to scaled pseudo ground accelerations due to seven separated ground motions. The ground motions are forced on the system in both directions where NovaFrame chooses the most unfavorable responses as the force demand. It is important to take both directions into account since each direction can give a different accumulation of forces where the element sections are exposed to. This is illustrated in the following figure 53.

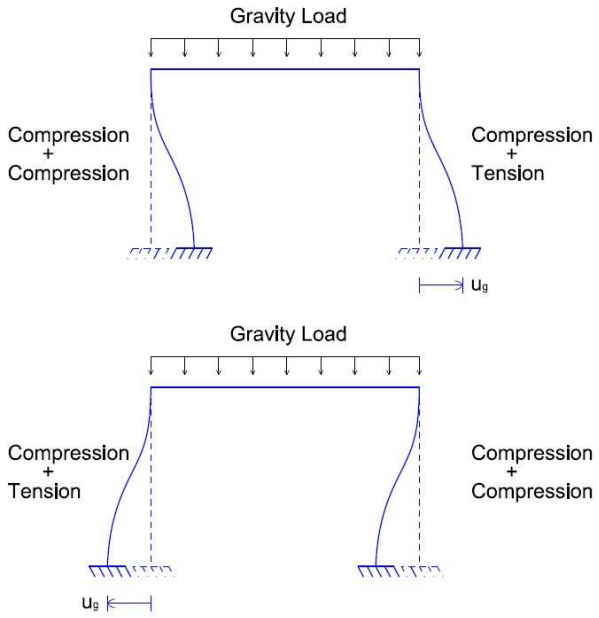

Figure 52 - Force accumulation due to different earthquake directions

For an overall view of the models for both designs and their notations see figures 43 and 44.

RSA, Results and Discussion of Design 1, Longitudinal

In the following charts section moments for towers and caissons obtained by RSA for the seven ground motions are presented. The charts also show a comparison between sections in different towers or caissons denoted by element number and element end (e.g. 756_1) where the first digit of the element number also represents the tower or caisson number and the last digit represents the element end.

In Figure 53 we can see that the section moments at top of the towers are identical for all the ground motions. These identical forces can be reasoned to the towers identical heights and elevation at the top and base.

Figure 54 shows the section moments at the base of the towers. We can observe that the results for the two towers are different but close when compared. These can be reasoned in the fact that Caisson 800 is higher than caisson 700.

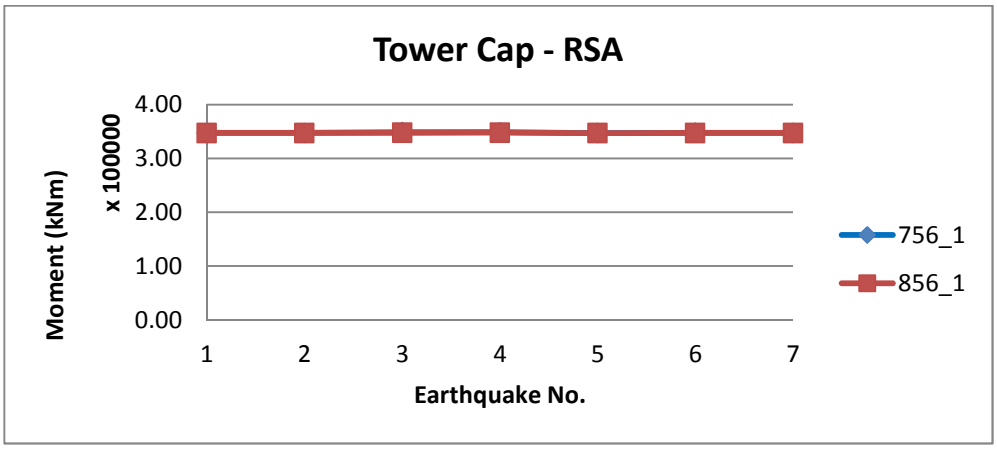

Figure 53 - Moment chart for design 1

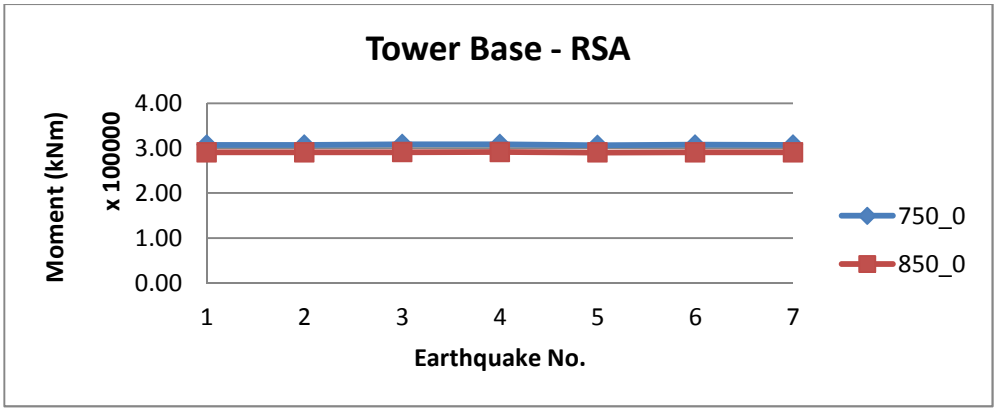

Figure 54 - Moment chart for design 1

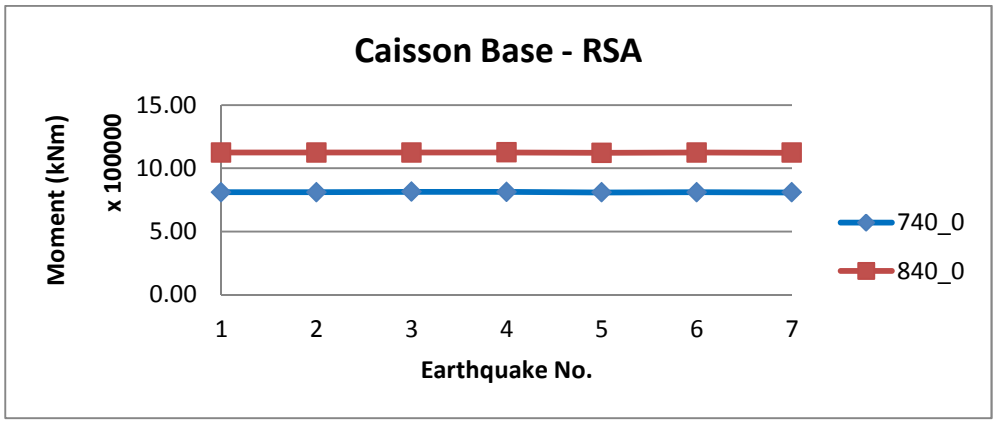

Figure 55 - Moment chart for design 1

Figure 55 shows the section moments at the base of the caissons. Here we can observe that the differences in forces between the two caissons are much larger than the other sections in the previous figures. This can be explained due to the total height of C800 which is higher than C700. The difference in height will affect the total force triangle and thus force different.

The preceding three figures show a straight line results. It means that moments do not change during different earthquakes. This can be explained by studying the mass participation factor at Table 1. The scaled response spectrum for each earthquake gives the same spectral accelerations for the first mode while the spectral acceleration given for the rest of the modes can be different. This is due to the fact that all ground motions are scaled with respect to only the first mode. From Table 1 It can be seen that the mass participation of mode 1is above 99%. This indicates that, the rest of the modes contribute with less the 1% to the total response. This explains why the results are the same by 99%. The same conclusion applies for the displacements.

A comparison of displacements of the two towers due to the ground motions are plotted in Figure 56. The largest displacements occur at the top of the towers and hence the top sections will be compared.

The first behavior to notice is the difference in displaced direction between the towers. The logical assumption would be to think that both towers should be displaced in the same direction since the same ground motion is applied at the base of all supports. This means that all the bridge components should move forth and back simultaneously. Since there are only two types of loading applied on the designs it is safe to conclude that the gravity loading is much more dominant than the seismic loading. As mentioned in chapter 5, it is only the towers that resist the longitudinal displacements while the columns act only as vertical support without prohibiting longitudinal displacements. This means that the pulling forces due to the superstructure's dead weight are much larger towards the ends of the bridge than the center of the bridge. It can also be observed that the displacements are slightly larger towards the right direction at tower 800 compering to displacement at left direction at tower 700. This is because the gravity load is much larger at the right side of tower 800 due to a larger beam section and hence larger pulling force.

These observations confirm that the seismic loading is very moderate or low.

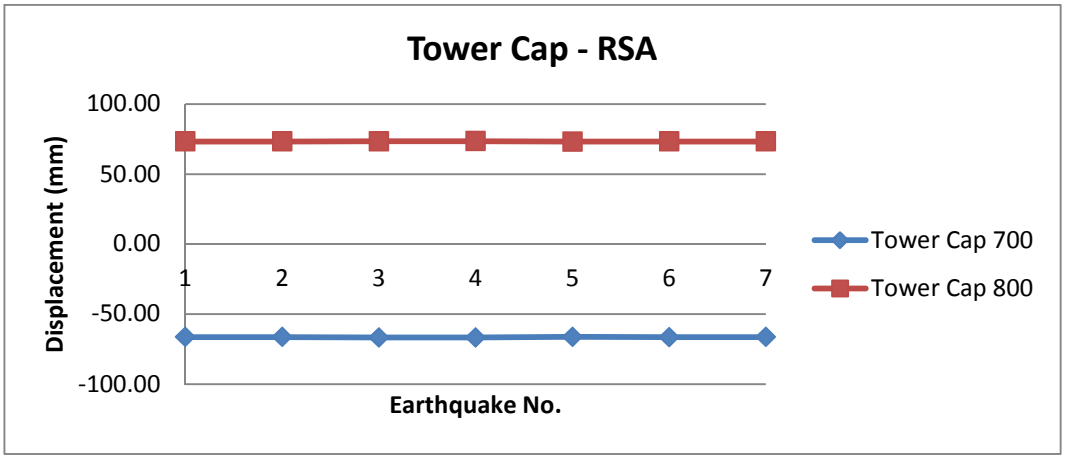

Figure 56 - Displacement chart for design 1

RSA, Results and Discussion of Design 2, Longitudinal

Figure 57 shows clearly that magnitudes of moments are much higher at the top of tower 400 and tower 900 where these also are the outer towers. As in design 1, these outer towers have a larger share of forces due to the gravity loads of the beam sections. And as expected as tower 400 supports a larger beam section it is also exposed to larger moments compared to tower 900. Again, this means that loads due to gravity are the dominant ones compared to seismic loading.

The same conclusion can be made for Figure 58 and Figure 59 as Figure 57.

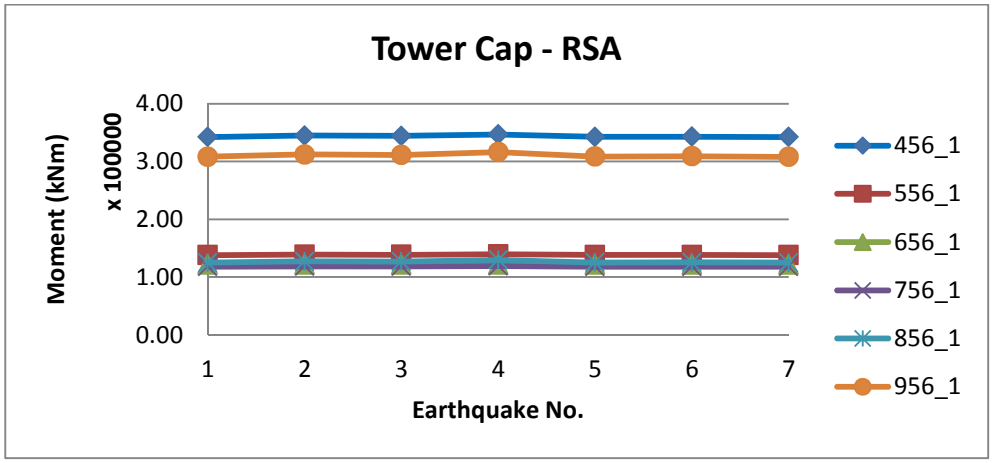

Figure 57 - Moment chart for design 2

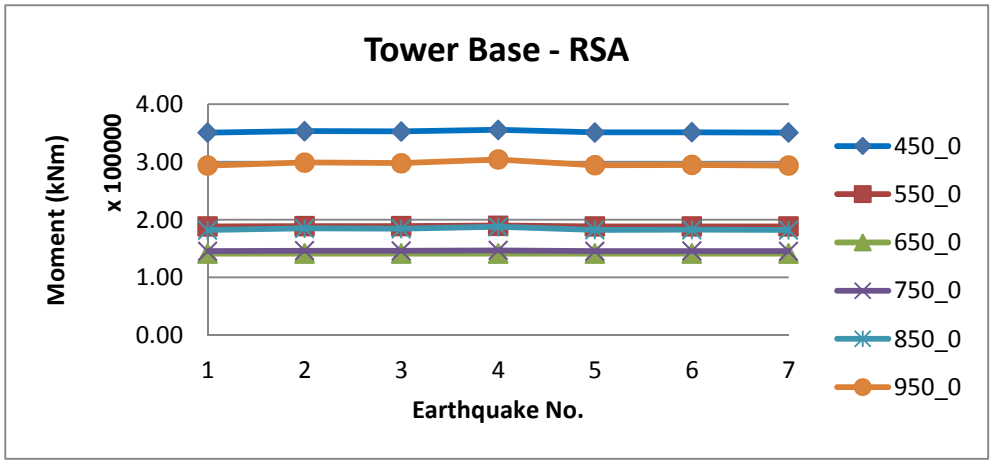

Figure 58 - Moment chart for design 2

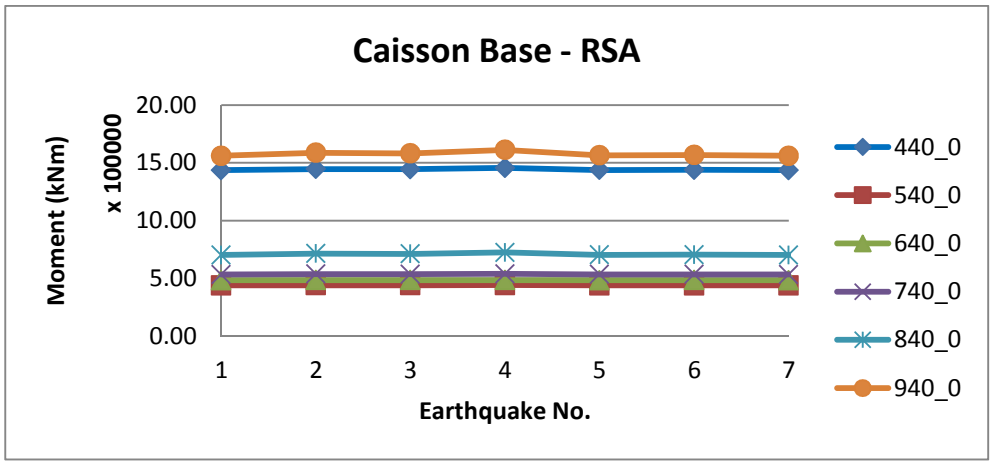

Figure 59 - Moment chart for design 2

Figure 60 shows the displacement chart in the longitudinal direction at top of the towers for design 2. We can see that the towers are divided into two groups in terms of direction. The split occurs in the middle of span 600 where all the towers on the left side are displaced towards left and all the towers on the right side are displaced toward right. It can also be observed that tower displacements towards the left side are larger than the other longitudinal direction. This is a conformation of the moment results and is due to same reason discussed for Figure 57, Figure 58 and Figure 59.

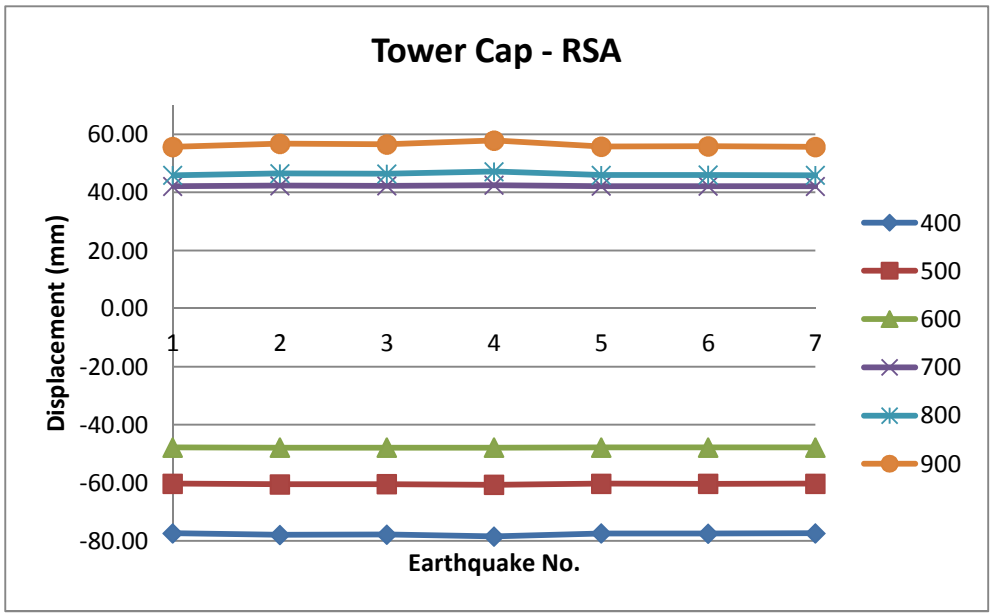

Figure 60 - Displacement chart for design 2

5.4 Elastic Time History Analysis (THA) in Longitudinal Direction

This section presents results of the THA performed for both of the bridge designs. The aim is to evaluate the responses of the two designs and get a good overview of the bridges behavior exposed to seven different ground motions at separate times. These are the same ground motions presented earlier in section 5.3.1which also were used in RSA. All he ground motions are scaled according to section 5.3.4.

5.4.1 THA in OpenSees

The THA in OpenSees is performed under the horizontal ground motions. OpenSees uses Newmark's integration method where the unconditional stability are satisfied for $\beta = 0.25$ and $\gamma = 0.5$. As for the RSA, the damping ratio is sat to $\zeta = 5.0\%$ where the Rayleigh damping is applied for assembling of the classical damping matrix. The Rayleigh parameters a_1 and a_2 are determined using the first and the second mode in horizontal direction respectively. The time steps and recording durations are different for all the ground motions and hence individual values are used for every ground motion.

5.4.2 Results and Discussion of THA in Longitudinal Direction

As for the RSA, the section forces that are evaluated are top of the towers, base of the towers and base of the caissons. In the following, moments and displacements in the longitudinal directions are plotted in different charts for comparison.

THA, Results and Discussion of Design 1, Longitudinal

Figure 61 shows equal moments at top of both towers during earthquake 1 to 3. For the remaining earthquakes the results are still very close to each other.

The same pattern is shown in Figure 62 and Figure 63 as the previous figure. Figure 63 also shows that caisson 800 has higher moments at its base.

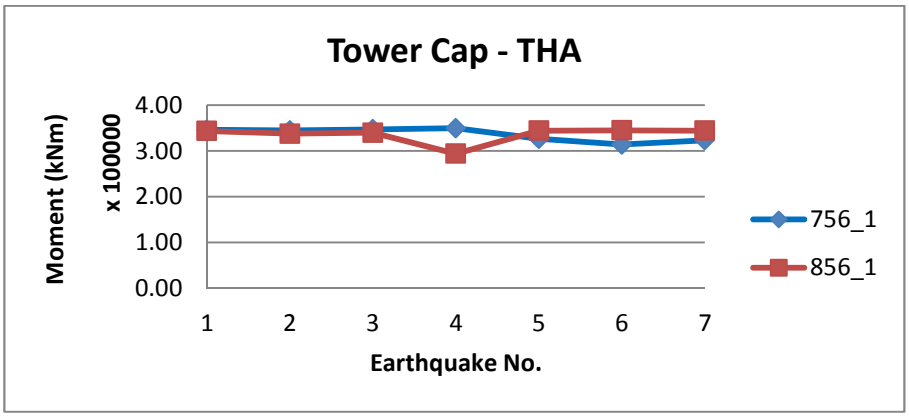

Figure 61 - Moment chart for design 1

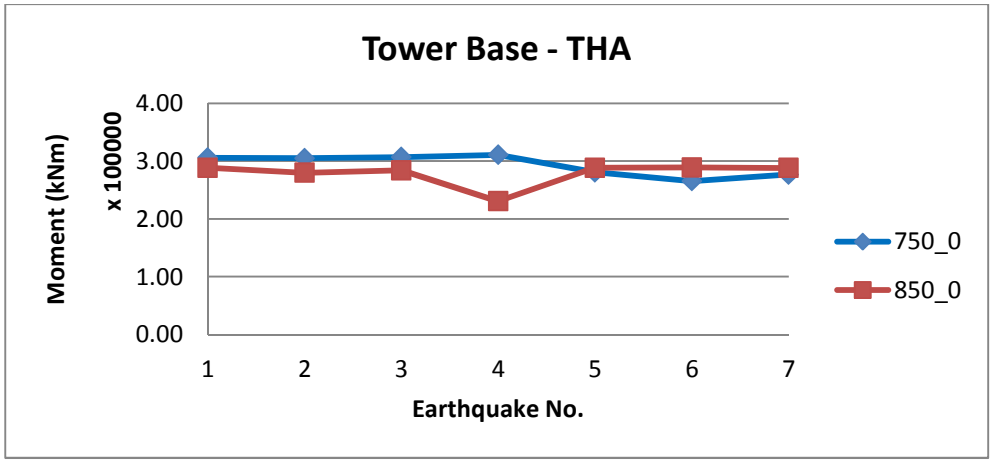

Figure 62 - Moment chart for design 1

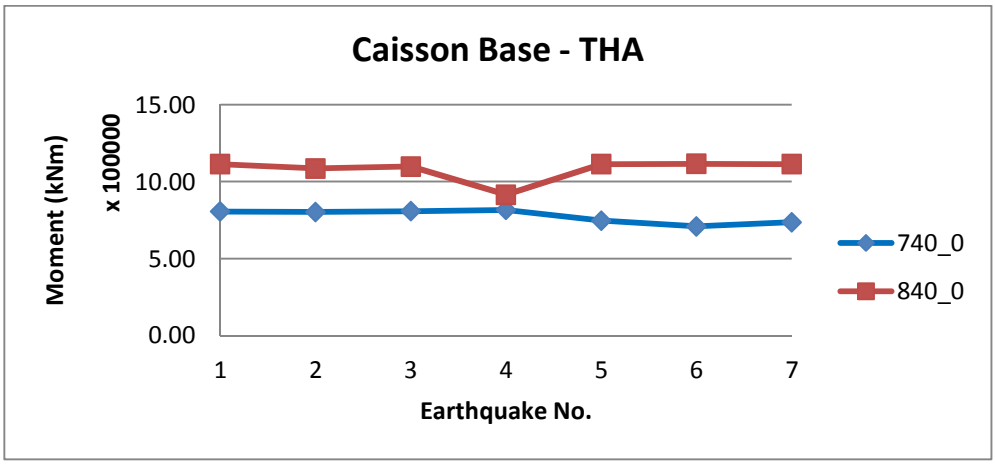

Figure 63 - Moment chart for design 1

The displacement at the top of the towers in Figure 64 confirms the same pattern as for the RSA. The two towers are displaced in opposite direction due to gravity of the beam sections which play the dominant load role.

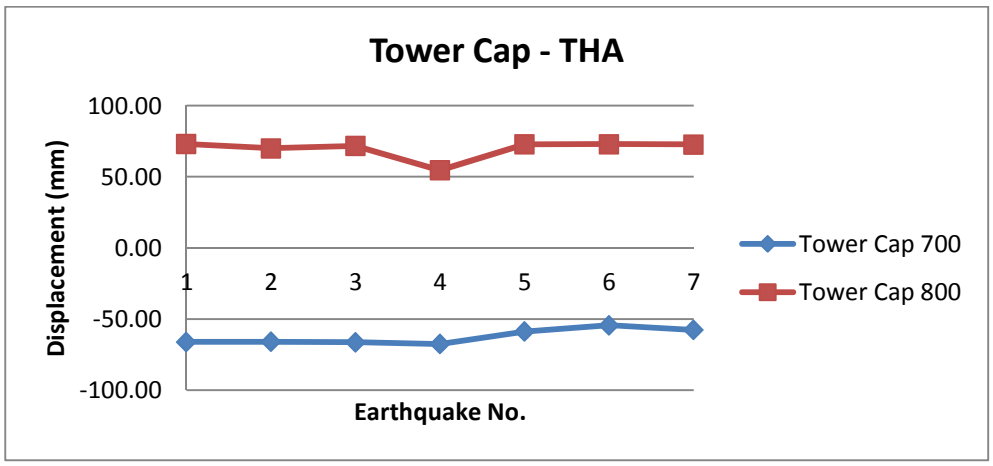

Figure 64 - Displacement chart for design 1

THA, Results and Discussion of Design 2, Longitudinal

As for the RSA, Figure 65 and Figure 66 shows that the two towers which stand out in term of highest moments are the outer towers where tower 400 has the most highest forces. This is also true for the base of caissons in Figure 67 except that caisson base 900 is exposed to the highest moments.

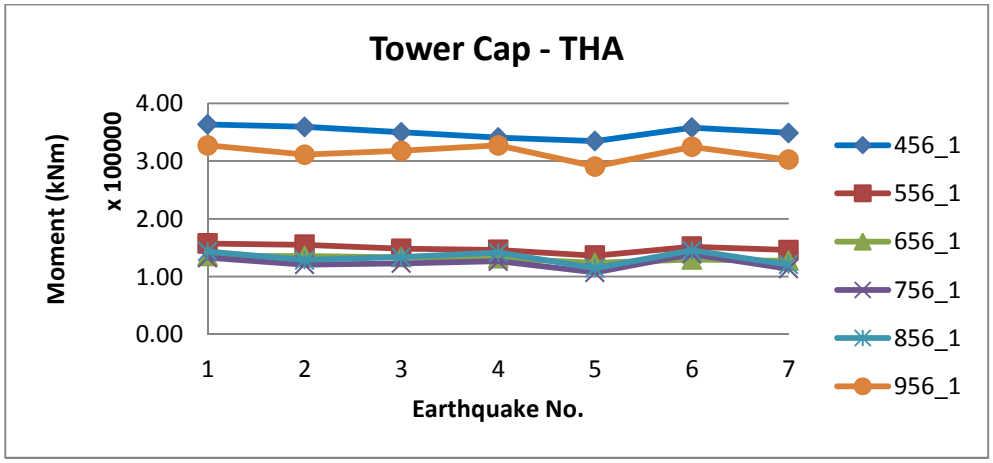

Figure 65 - Moment chart for design 2

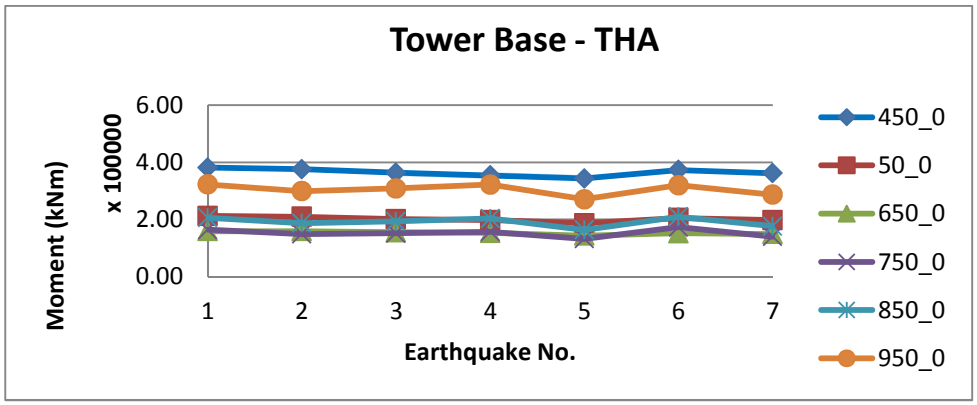

Figure 66, moment chart for design 2

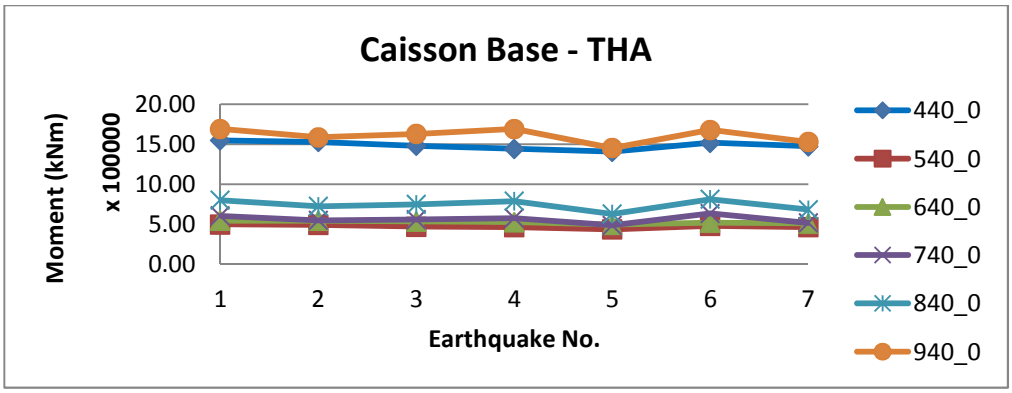

Figure 67, moment chart for design 2

Figure 68 shows the longitudinal displacement at the top of the towers. We get the same pattern here as for the RSA where towers on the right side of span 600 are displaced toward right while towers on the left side of span 600 are displaced toward left in the longitudinal direction. It can also be seen that the outer towers have the highest displacements where tower 400 is displaced most. This is the same result as in the RSA.

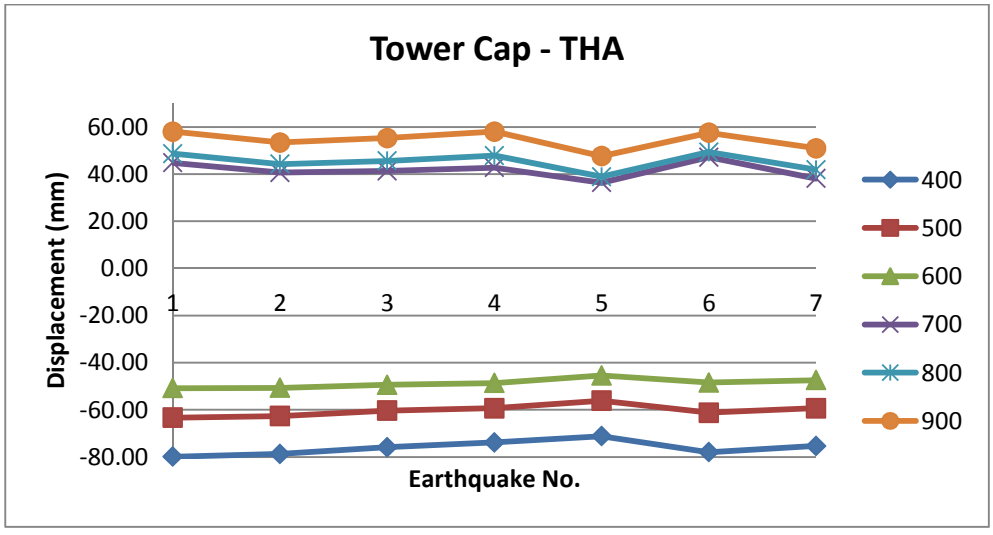

Figure 68, displacement chart for design 2

5.5 Comparison and Discussion Between RSA, THA and DSA in Longitudinal Direction

In the following sections a comparison of different analysis methods between RSA, THA and design spectrum analysis (DSA) are presented. A tower with the most significant responses is selected for each design where the results by different method of analysis are to be compared.

The DSA is performed by NovaFrame where the DS obtained in section 5.3.3 is used.

5.5.1 RSA Versus THA for Design 1, Longitudinal

Section moments of tower 800 obtained by different analysis methods under seven ground motions are compared in Figure 69, Figure 70 and Figure 71. We can observe that the RSA values are almost the same as the THA values for six of the seven earthquakes where a difference is standing out for earthquake number 4. As mentioned before, for the longitudinal analysis NovaFrame needs only one mode to get a participation factor above 99% and three modes to reach 100%. While THA takes all the modes in to account. In Figure 50one of the scaled RSs are standing out by reaching a magnitude of above 7.0 g. This is actually the spectral acceleration for earthquake number four which is scaled up to meet the DS at the first mode of bridge design 1, that is at $T_1 = 2.05$. As the difference between the spectral accelerations at different periods increases we will observe a bigger deviation between RSA and THA where the THA is the most accurate one. Except that most of the response contribution in the RSA is due to the first mode in this case, NovaFrame uses only ten spectral ordinates from the scaled RS to create its own RS with smooth lines. This means that 10 points are not enough to catch all the peaks at different periods and hence we can observe an almost straight line for the RSA while THA gives the exact results.

When comparing the RSA and the THA against the DSA we can observe that DSA gives the lowest force demands. This is as expected since DSA has the aim of pushing the structure to and above the yielding point. In other words DSA wants to apply some damage to predetermined points at the structure to prevent total collapse.

Another interesting observation is that DSA has managed to set earthquake number four above the force demand value at all element sections.

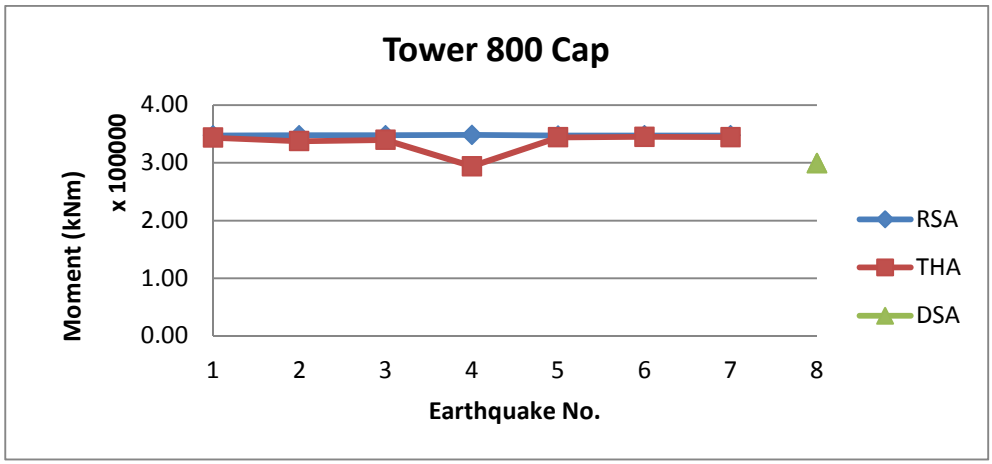

Figure 69- Moment chart for design 1

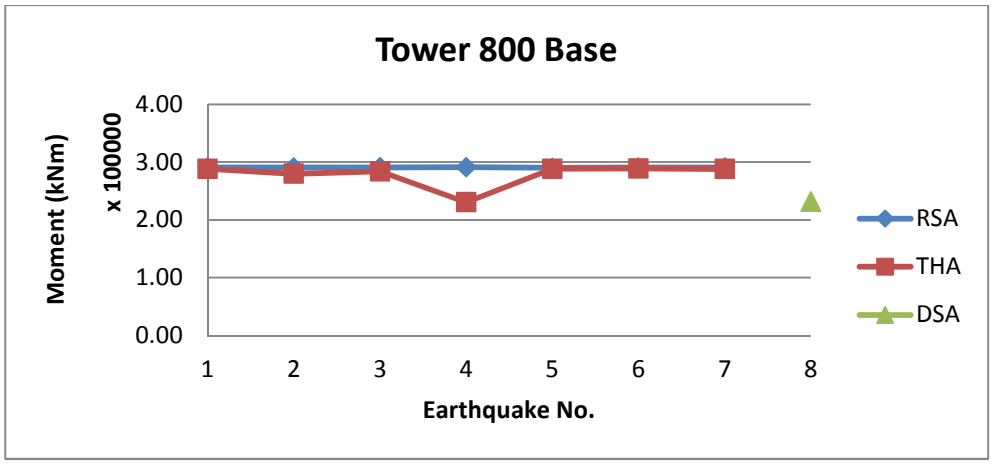

Figure 70 - Moment chart for design 1

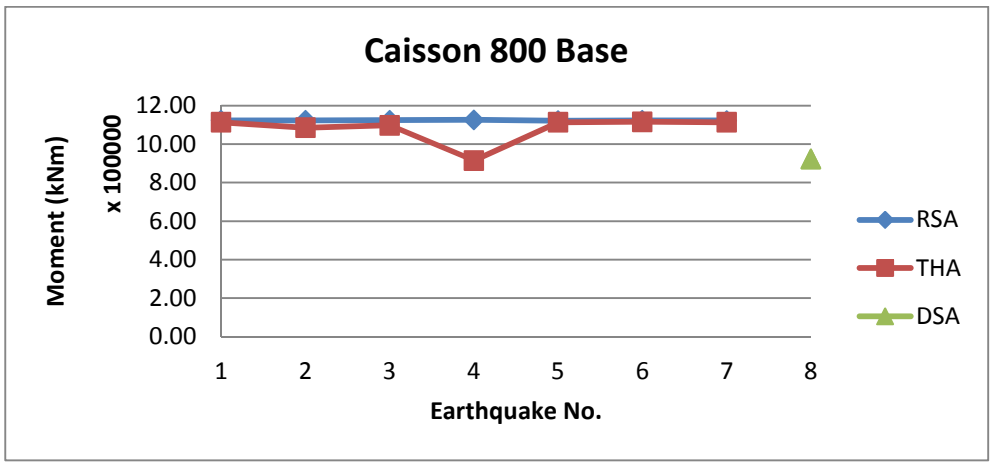

Figure 71 - Moment chart for design 1

Figure 72 shows the longitudinal displacement by different analysis methods. The same pattern as for the moment charts in Figure 69, Figure 70 and Figure 71 can be observed. We can also see that the RSA has been the most conservative method with respect to both moments and displacements. The DSA gives the lowest displacements due to the q factor.

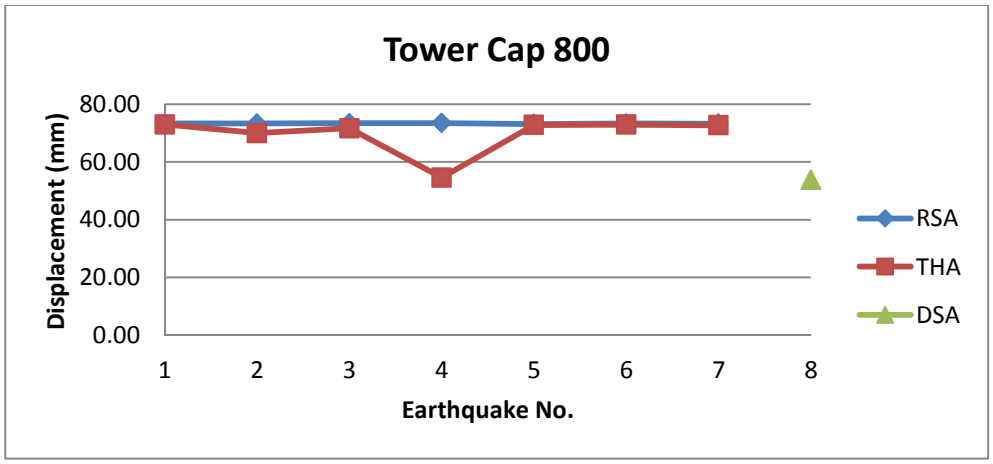

Figure 72 - Displacement chart for design 1

5.5.2 RSA Versus THA for Design 2, Longitudinal

In Figure 73, Figure 74 and Figure 75, we can observe very close results between RSA and THA and in some cases almost identical. Design 2 doesn't have the same deviation under earthquake number four. This may be due to a much closer space between the first and the second mode compared to design 1. We can also observe that the RSA is not the most conservative one.

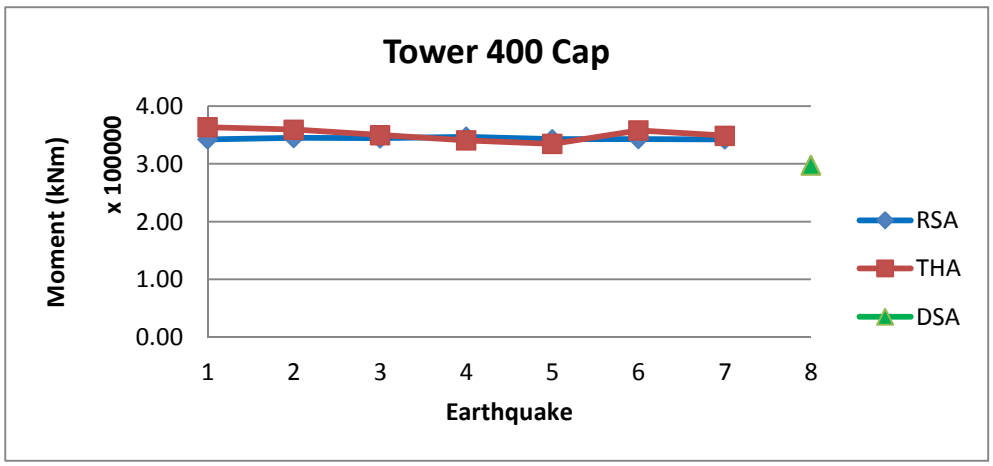

Figure 73 - Moment chart for design 2

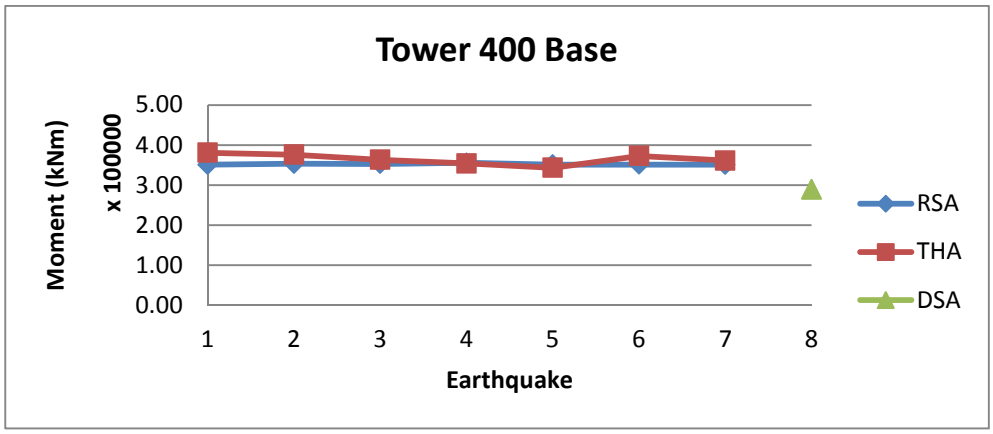

Figure 74 - Moment chart for design 2

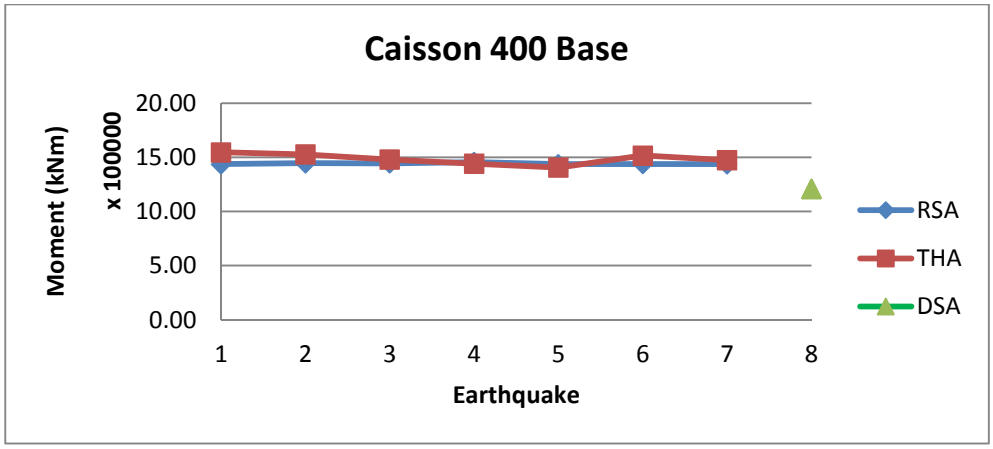

Figure 75 - Moment chart for design 2

Figure 76 shows the longitudinal displacement of tower top 400 by different methods of analysis. Close displacement values can be observed for RSA and THA. The DSA gives a lower displacement as expected.

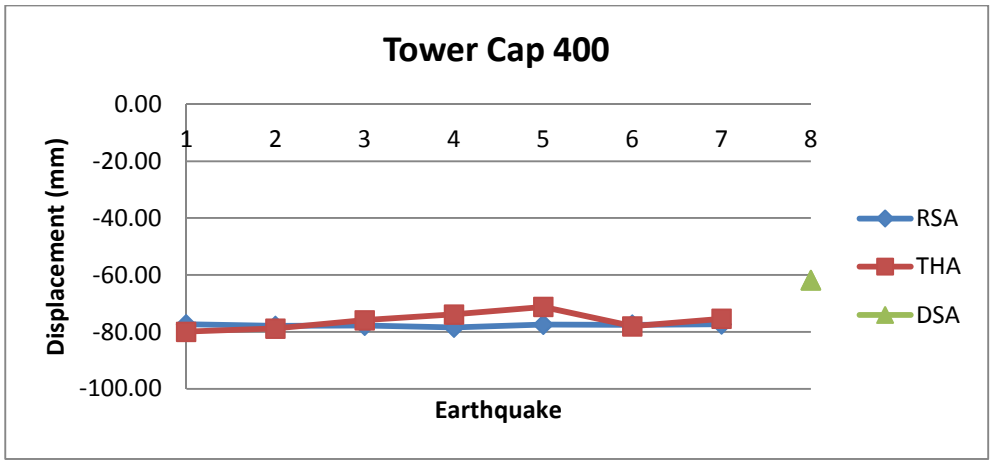

Figure 76 - Displacement chart for design 2

6 Numerical Analysis and Discussion of Results (Transverse)

6.1 Introduction

In this chapter, the two bridge designs were analyzed by using RSA. First the eigenvalues were determined then the responses were computed. The results were plotted and compared.

6.2 Eigenvalue Analysis (EVA) in Transverse Direction

6.2.1 Results of Eigenvalue Analysis (EVA) in Transverse Direction

For the transverse direction RSA needed up to 10 modes to obtain a participation factor of above 90%. Table 5 shows the eigenvalue results for design 1 in term of natural cyclic frequency and natural periods. The participation factors are also listed for every mode.

Unlike RSA for the longitudinal direction, we can observe the need of many more modes and the contribution of higher modes to the total response. Some of the modes are excluded from Table 5 since because of zero participation.

Figure 77 shows the three first mode shapes of design 1.

Table 5 - Natural frequency and period of design 1, transversal

Design 1 **Novaframe**

	Modal participation	Natural cyclic frequency	Natural period
	%	f, Hz	T, s
Mode 1	0.375	0.703	1.42
Mode 2	0.063	0.922	1.08
Mode 3	0.198	1.010	0.99
Mode 4	0.052	1.144	0.87
Mode 5	0.093	1.361	0.73
Mode 7	0.05	1.461	0.68
Mode 9	0.052	1.615	0.62
Mode 11	0.021	1.834	0.55
Mode 13	0.018	1.982	0.50
Mode 15	0.016	2.181	0.46

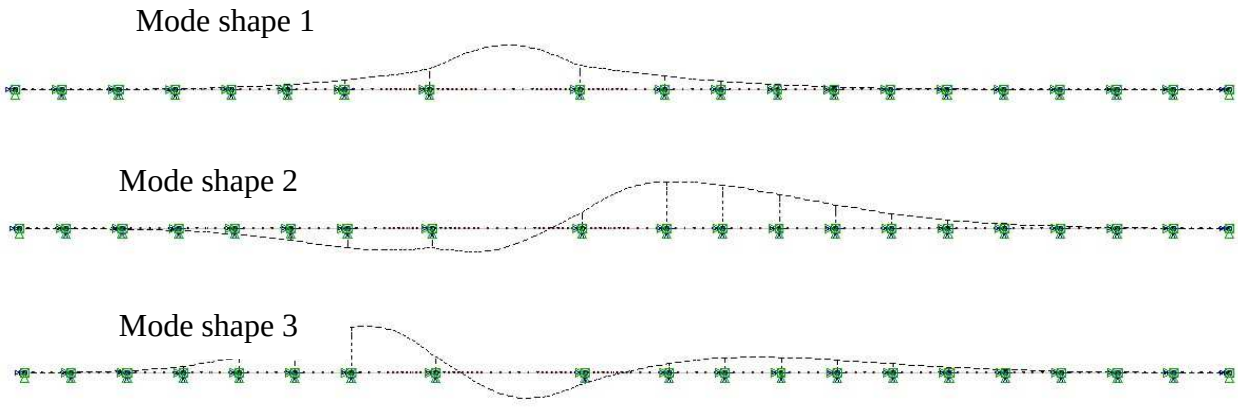

Figure 77 - Mode shape 1, 2 and 3 of design 1, transverse direction

Table 6 shows the eigenvalue results for design 2 in transverse direction. As for the design 1, up to 10 modes are needed to reach a mass participation of above 90%. Figure 78 shows the first three mode shapes of design 2 in transverse direction.

Table 6, Natural frequency and period of design 2, transversal

Design 2			**Novaframe**
	Modal participation	Natural cyclic frequency	Natural period
	%	f, Hz	T, s
Mode 1	0.451	0.661	1.51
Mode 3	0.126	0.808	1.24
Mode 4	0.009	0.823	1.22
Mode 5	0.117	0.887	1.13
Mode 6	0.087	1.287	0.78
Mode 7	0.1	1.359	0.74
Mode 9	0.007	1.765	0.57
Mode 11	0.036	2.129	0.47
Mode 13	0.008	2.421	0.41
Mode 15	0.023	3.122	0.32

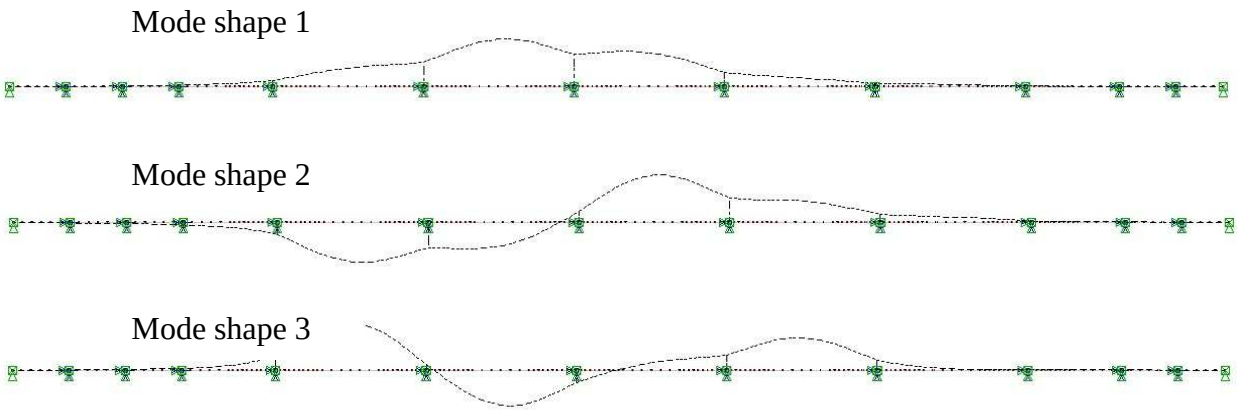

Figure 78 - Mode shape 1, 2 and 3 of design 2, transversal

6.2.2 Discussion of Results (EVA), Transvers

Comparing the results of the two designs shows a much closer frequency between the designs compared to the longitudinal direction. The closeness of frequencies indicates that the designs behave very much alike in transverse direction. The fact that up to 10 modes are needed to get the necessary mass participation makes very much sense since the mass movement in different direction at varies times is much less synchronized.

6.3 Elastic Response Spectrum Analysis (RSA) in Transversal Direction

6.3.1 Scaled Ground Motion in Longitudinal Direction

As for the longitudinal direction the response spectrum of each ground motion were scaled down using the first mode in transverse direction to meet the design spectrums spectral acceleration at the same mode. Table 7 scaling factor values for each design in transverse direction for all ground motions.

Table 7 - Scaling factor values for transversal direction

		Design 1			Design 2		
	T_mode 1 EarthQuakes	S_e RS	S_e DS	1.42 Scaling Factor	S_e RS	S_e DS	1.51 Scaling Factor
1	Coyote Lake	0.0971	0.1213	1.250	0.1062	0.1132	1.066
2	Gulf of California	0.0136	0.1213	8.913	0.0133	0.1132	8.513
3	Imperial Valley-07 1979	0.0110	0.1213	10.998	0.0091	0.1132	12.384
4	Northridge-06	0.0045	0.1213	26.808	0.0039	0.1132	28.875
5	Westmorland	0.0825	0.1213	1.470	0.0769	0.1132	1.473
6	Whittier Narrows-01	0.0626	0.1213	1.937	0.0528	0.1132	2.143
7	Yountville	0.0028	0.1213	43.385	0.0023	0.1132	49.766

6.3.2 Results and Discussion of RSA in Transversal Direction

The moments and displacements for selected tower and caisson sections of the two designs are plotted in charts for all the ground motions. Then the results are compared and evaluated. The charts show a comparison between sections in different towers or caissons denoted by element number and element end (e.g. 756_1) where the first digit of the element number also represents the tower or caisson number and the last digit represents the element end.

RSA, Results and Discussion of Design 1, Transversal

Figure 79, Figure 80 and Figure 81 shows the moments of all the towers and caisson for given sections. Unlike the results for the longitudinal direction, the results do not show a straight line. The reason is that the total response is due to several mode contributions and not just the first mode. Thus, design one react much more differently due to different earthquakes.

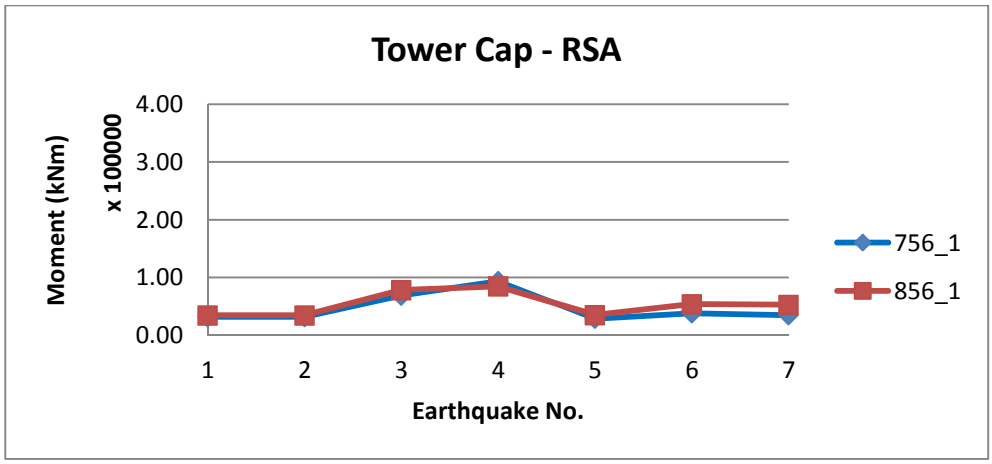

Figure 79 - Moment chart for design 1

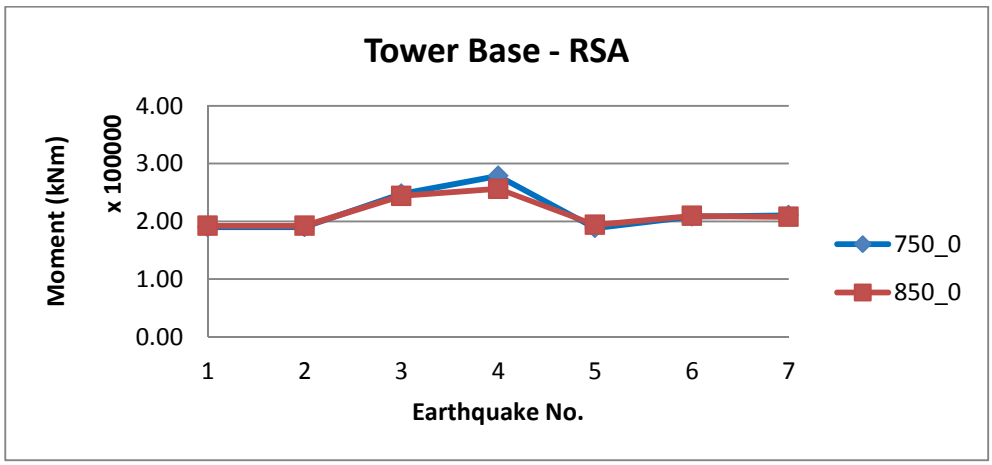

Figure 80 - Moment chart for design 1

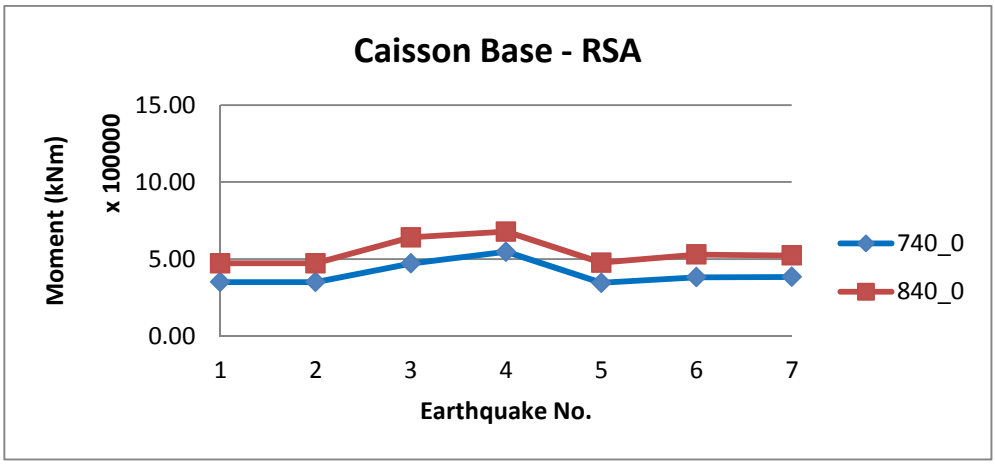

Figure 81 - Moment chart for design 1

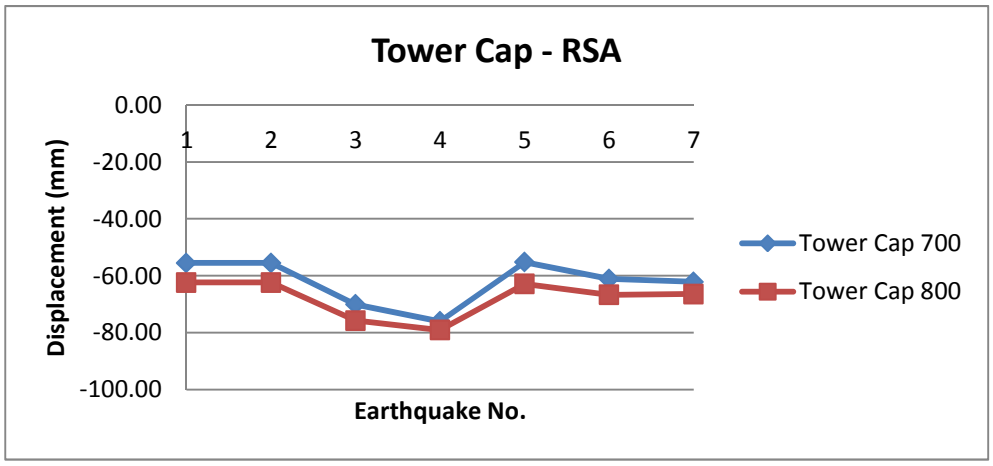

Figure 82 - Displacement chart for design 1

In the same way as for Figure 79, Figure 80 and Figure 81, the displacement has a significant variation when exposed to different earthquake. The displacements of both towers are in the same directions since the gravity loads do not have a big effect in transverse direction as for the longitudinal.

RSA, Results and Discussion of Design 2, Transversal

The contribution of many more nodes compared to longitudinal directions much more apparent in Figure 83, Figure 84 and Figure 85. It can also be observed from Figure 83 that the outer towers do not have the highest moments regarding to the tower cap. We can also conclude that earthquake is the dominant load in transverse direction due to the variety of the results.

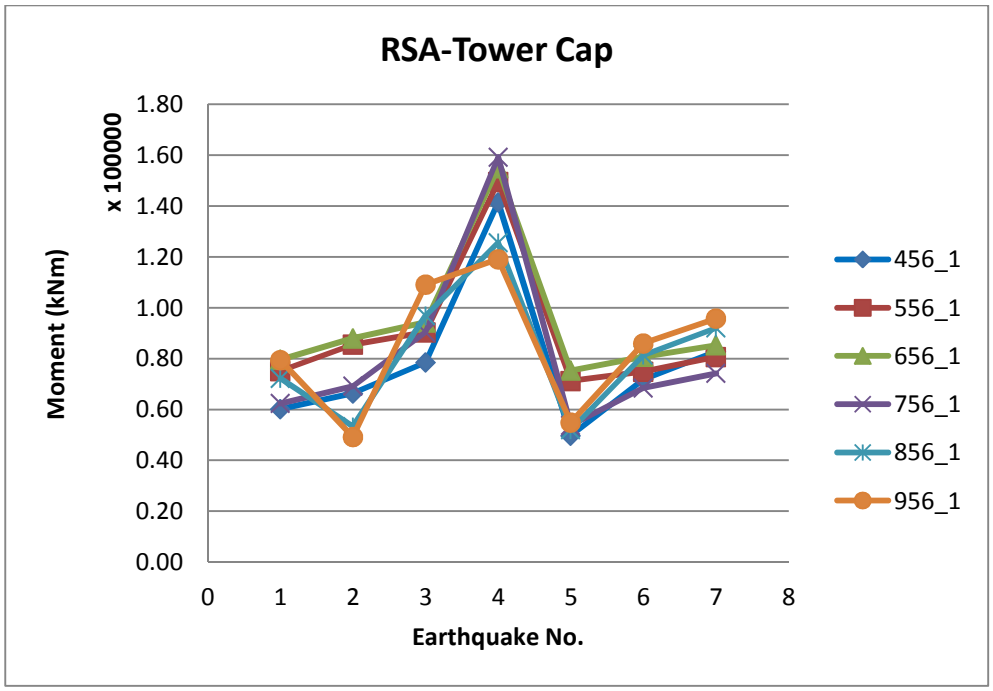

Figure 83 - Moment chart for design 2

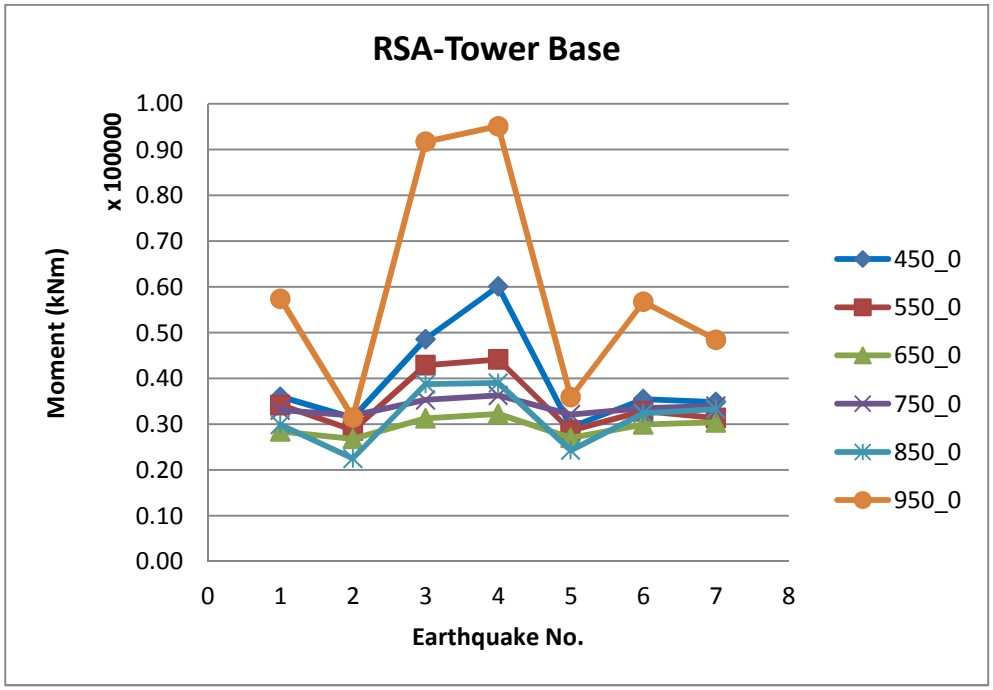

Figure 84 - Moment chart for design 2

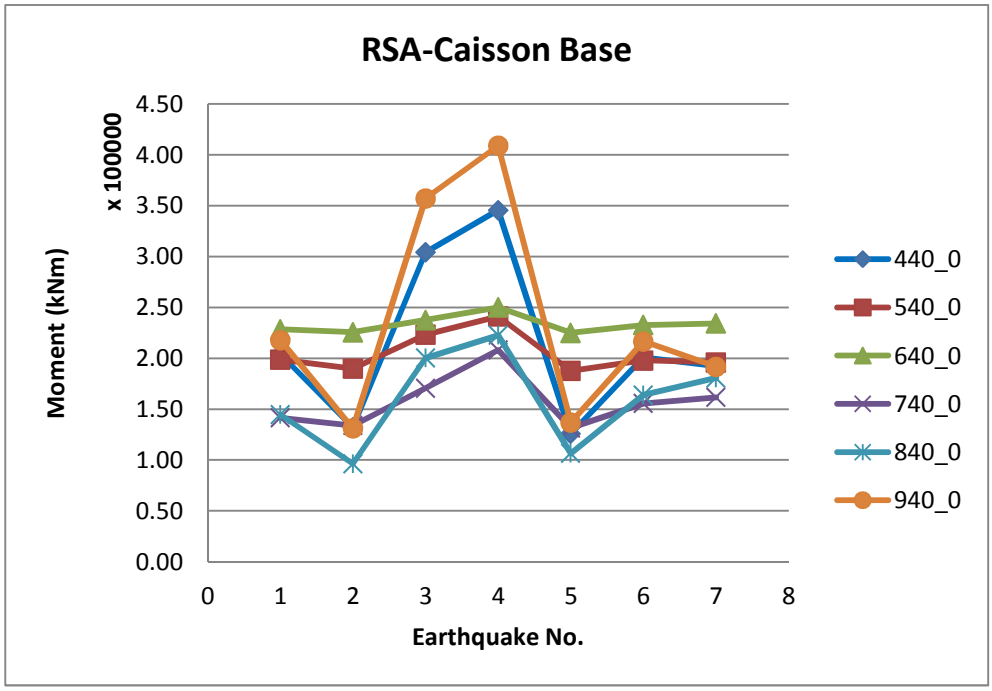

Figure 85 - Moment chart for design 2

Figure 86 shows the displacement in the same direction. This is expected since the earthquake excitation plays the dominant loading role. Design 2 has larger displacements compared to design 1, specially tower 600 under earthquake number three and four.

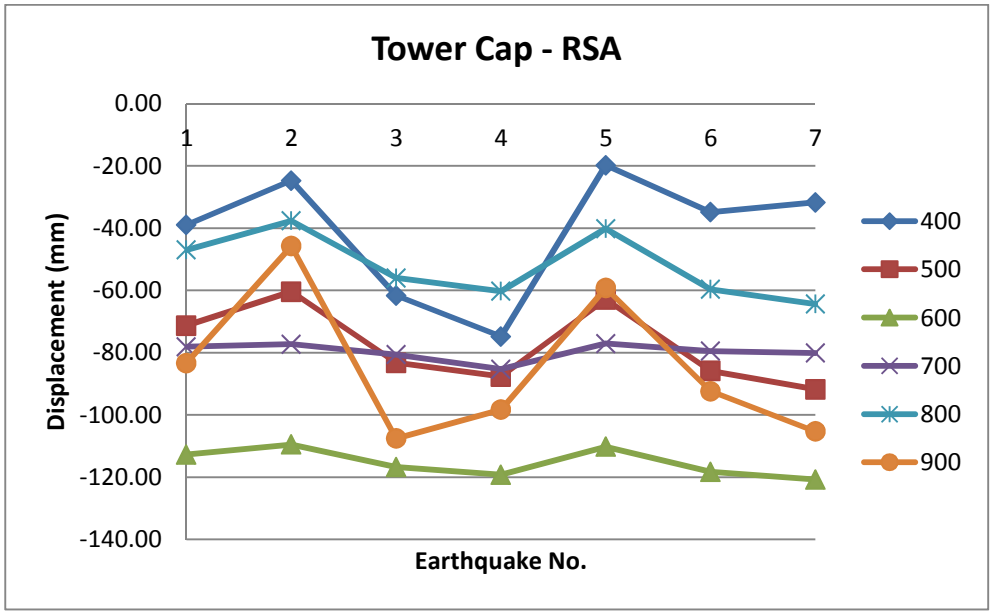

Figure 86 - Displacement chart for design 2

7 Comparative Response Evaluation of two Designs

7.1 Introduction

The aim of this chapter is to do a comparison between bridge design 1 and 2 with respect to seismic performance. The main purpose is to conclude which of these designs are the better alternative to withstand an earthquake excitation.

The Chapter starts with a demand capacity ratio (DCR) assessment of both designs in longitudinal and transverse direction where the results were compared. This will give us an overview of how prone these designs are to damages induced by ground motions. Next it will be shown which of these designs have the highest displacements. Then the Chapter ends with an overall discussion.

7.2 Demand Capacity Ratio Assessment in Longitudinal Direction

The moment demands from the THA by OpenSees are compared to the strength capacity of tower and caisson sections designed in NovaFrame with respect to the design spectrum. The ratio of this comparison is called demand capacity ratio which is permitted to exceed unity to a certain point where ductile response is assured. The DSA method's aim is to reduce the actual force demand by using the q factor approach and use the reduced demand for designing the bridge sections. By doing so, we will allow some controlled damage to the bridge which is also called ductile behavior. By performing a DCR assessment to different tower and caisson sections we can get a measure of how ductile these members are. This is done by comparing the real capacity without the use of any material factors to the real force demand obtained by THA without the use of the q factor.

The DCR value should be $0 < \text{DCR} < 1.5$.

Figure 87 shows the DCR of design 1 at the element sections of tower700, tower 800 and their caissons. It can be observed that all the DCR values are below 1.15 where the acceptable ratios are < 1.5.

Figure 88 shows the DCR for design 2 at element the sections of tower400 to tower 900 and their caissons. In the same way as in Figure 87, Figure 88 also shows acceptable values where all the DCRs are smaller than 1.5. However the overall values are somewhat higher for design 2 than for design 1.

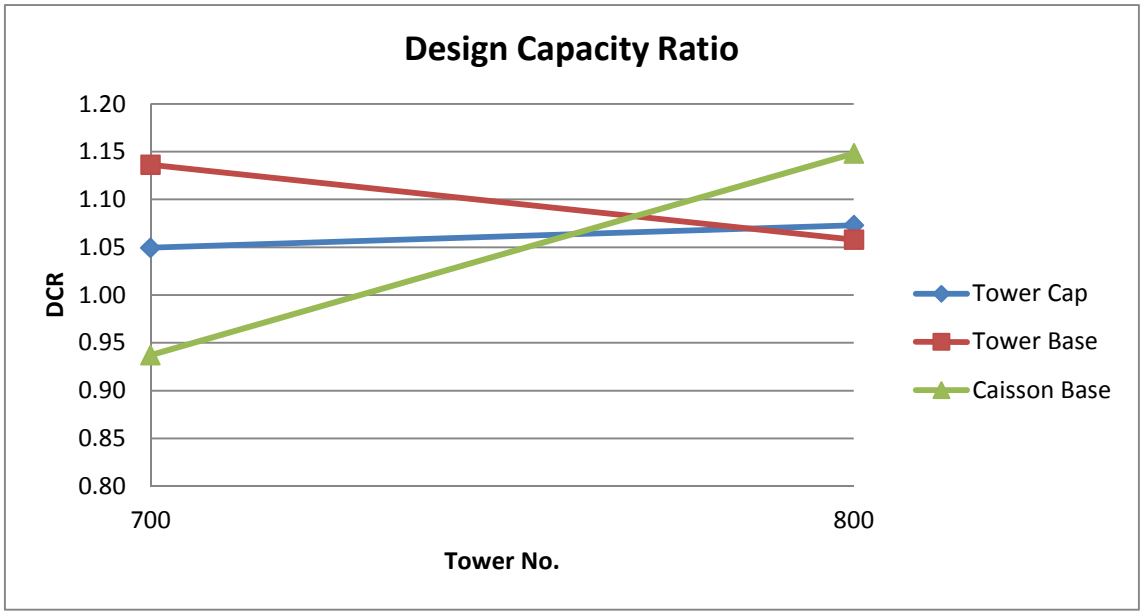

Figure 87 - Design Capacity Ratio for design 1, longitudinal

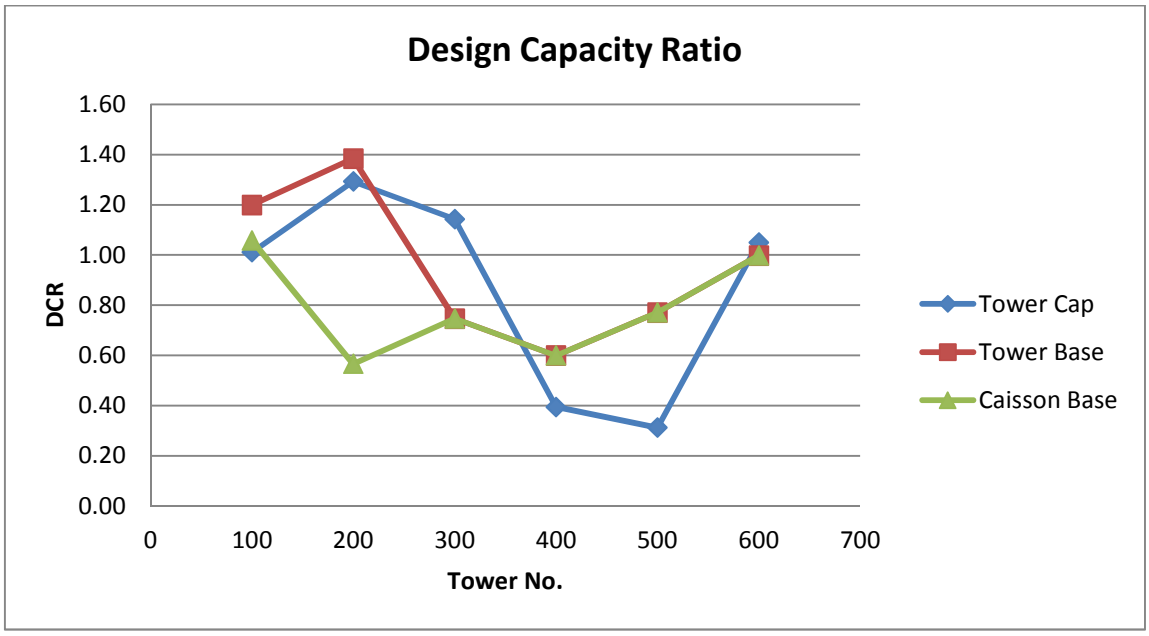

Figure 88 - Design Capacity Ratio for design 2, longitudinal

7.3 Demand Capacity Ratio Assessment in Transversal Direction

Unlike the longitudinal direction, forces obtained by the RSA were used as the force demand and compared to the section strength designed by the DSA.

Figure 89 shows the DCR values of design 1 for both towers and their caissons in transverse direction. A high stiffness can be observed for all the sections where DCR is safe below 1.5.

Figure 90 shows calculated DCR values for design 2. It can be observed that tower400 is the least rigid tower at its cap and base. However the DCR values are safely below the limit.

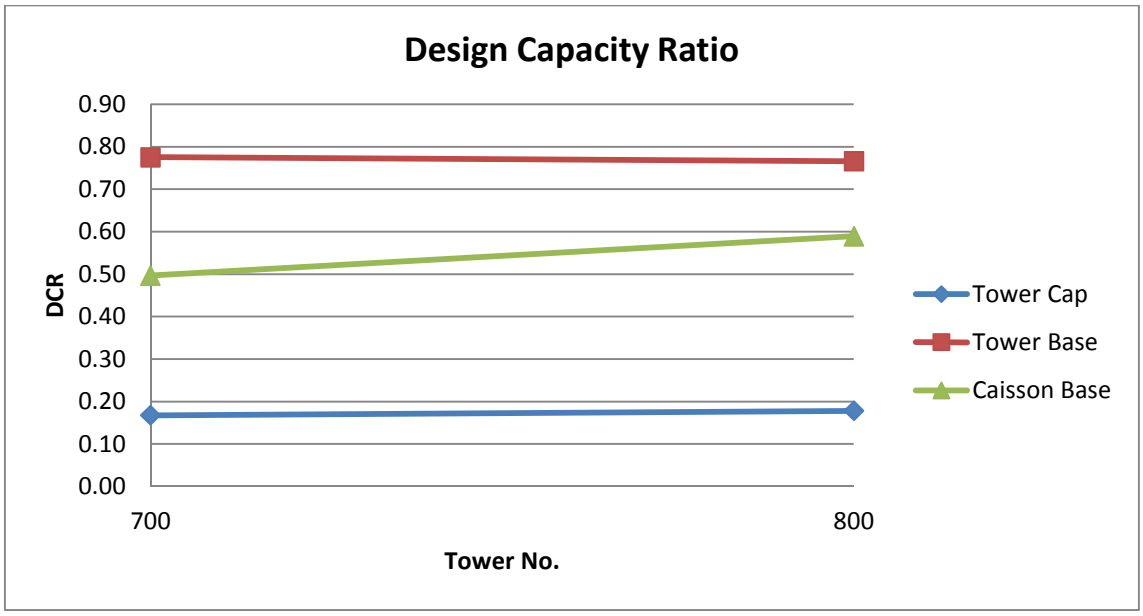

Figure 89 - Design Capacity Ratio for design 1, transversal

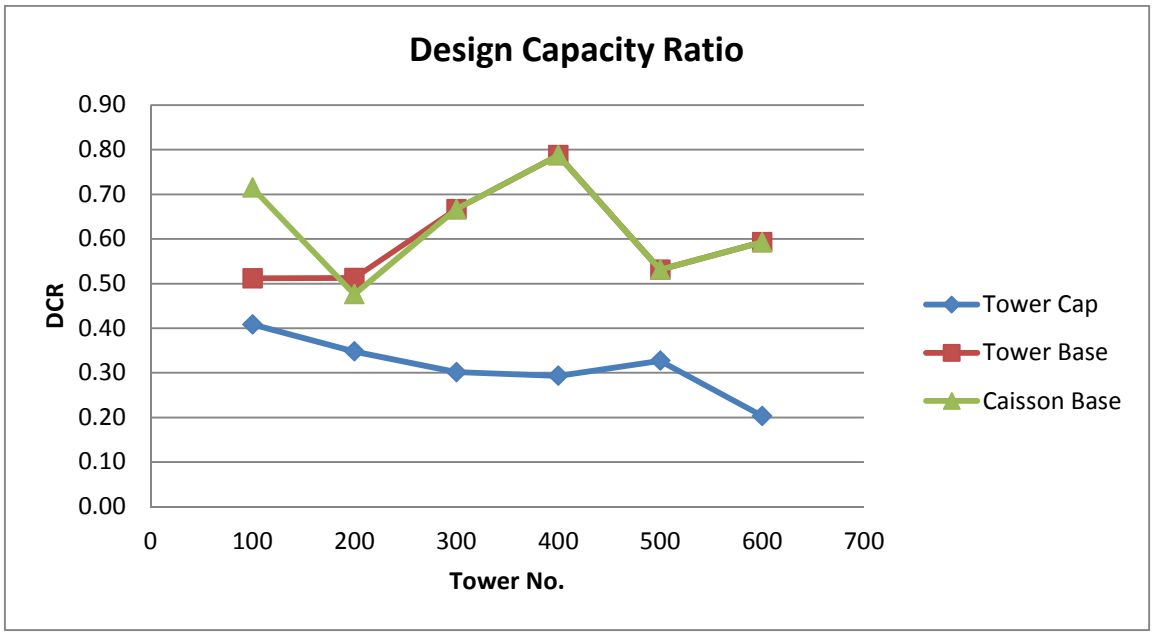

Figure 90 - Design Capacity Ratio for design 2, transversal

7.4 Discussion

The DCR results indicates that neither one of the designs will suffer damage that will force the bridges in to ductile behavior. However, design 2 seems to have the largest DCR values and could be the unfavorable one to ground motions that could exceed the design spectrum.

8 Conclusion

In longitudinal direction design 1 is a much more flexible structure with a natural period duration of 2.05 second which is 100% higher than design 2. This means that design 2 a much more rigid structure, longitudinal. A comparison of maximum moments and displacements that occurred in tower800 for design 1 and tower 400 of design 2 shows that design 2 is most exposed. While maximum displacement is approximately the same. This is unfortunate for design has a more demanding construction work.

In transverse direction the designs behave much more like each other with respect to duration of natural periods. Design 2 has a slightly larger period for the first mode with the largest mass participation which is due to the structural mass and not stiffness. This points out that a statically stiff structure is not necessary the right structure with respect to good behavior during an earthquake. Regarding to moment and displacements, design 1 is in front with an overall higher forces and displacement.

A comparison of DCR assessment in longitudinal direction shows that design 2 has an overall highest ratio. While in transverse direction the tower base of design 1 has the highest ratio which stays steady for both towers. While design 2 have a full tower, that is cap and base which is in the same ratio range as design 1.

Overall, design 1 has only one disadvantage compered o design 2, and that is in the transverse direction with higher response. But this can easily be overcome when the amount of construction work and complexity is much higher with design 2.

List of references

1) Anil K. Chopra, 2007. *Dynamics Of Structures: Theory and Applications to Earthquake Engineering,* Pearson Education, Upper Saddle River, New Jersey, Third edition.

2) Robert D. Cook, David S. Malkus, Michael E. Plesha, and Robert J. Witt, 2002. *Concepts and applications of finite element analysis,* John Wiley & Sons, Inc., Fourth edition.

3) Steven L. Kramer, 1996. *Geotechnical earthquake engineering,* Prentice Hall, Upper Saddle River, New Jersey.

4) M. J. N. Priestley, F. Seible, G. m. Calvi, 1996, *Seismic design and retrofit of bridges*, John Wiley & Sons, Inc., New York, Chichester, Brisbane, Toronto, Singapore.

5) Wai-Fah Chen, Lian Duan, 2003, *Bridge engineering: seismic design*, CRC Press LLC.

6) Dominik H. Lang, 2013, *Earthquake damage and loss assessment- predicting the unpredictable*, Dissertation for the doctor degree doctor philosophiae (Dr. philos), University of Bergen, Norway.

7) Dominik H Lang, 2004, *Damage potential of seismic ground motion considering local site effects,* Earthquake damage analysis center, Bauhaus- University Weimar.

8) Svein Ivar Sørensen, 2009, *Betongkonstruksjoner: Beregning og dimensjonering etter Eurocode 2*, Tapir akademisk forlag, Trondheim.

9) *Eurocode8: Design of structures for earthquake resistance, Part 1: General rules, seismic actions and rules for buildings (NA-EN 1998-1: 2004 + NA: 2008),* CEN: European committee for standardization, 2004.

10) *Eurocode8: Design of structures for earthquake resistance, Part 2: Bridges (NS-EN 1998-2: 2005 + A1:2009 + NA:2009),* CEN: European committee for standardization, 2005.

11) *NEED 2012: Norwegian earthquake engineering day 2012,* Norsk jordkjelvteknikk forening, Thon Hotel Vika Atrium, Oslo.